Membrane nanoclusters of FcRI segregate from inhibitory SIRP upon activation of human macrophages

DOI:
10.1083/jcb.201608094

Document Version
Accepted author manuscript

Membrane nanoclusters of FcγRI segregate from inhibitory SIRPα upon activation of human macrophages

Filipa B. Lopes[1,4], Štefan Bálint[1,4], Salvatore Valvo[2], James H. Felce[2], Edith M. Hessel[3], Michael L. Dustin[2], and Daniel M. Davis[1*]

[1]Manchester Collaborative Centre for Inflammation Research, University of Manchester, 46 Grafton Street, Manchester, M13 9NT, UK

[2]Kennedy Institute of Rheumatology, University of Oxford, Roosevelt Drive, Headington, Oxford OX3 7FY, UK

[3]Refractory Respiratory Inflammation Discovery Performance Unit, GlaxoSmithKline, Gunnels Wood Road, Stevenage, Hertfordshire, SG1 2NY, UK.

[4]These authors contributed equally

[*]Correspondence: Daniel M. Davis, Manchester Collaborative Centre for Inflammation Research, University of Manchester, 46 Grafton Street, Manchester, M13 9NT, UK. Tel: +44 (0)161 275 5019; E-mail: daniel.davis@manchester.ac.uk

Running title: Dynamics of FcγRI and SIRPα nanoclusters

Total character count (not including spaces): 43,940

eTOC blurb: Lopes et al. use super-resolution microscopy to visualize the nanoscale organization of activating and inhibitory receptors on human macrophages. Nanoclusters of inhibitory SIRPα and activating FcγRI associate in the cell's resting state but engagement of FcγRI induces their segregation.

Abstract

Signal integration between activating Fc receptors and inhibitory signal regulatory protein alpha (SIRPα) controls macrophage phagocytosis. Here, using dual-color direct stochastic optical reconstruction microscopy, we report that FcγRI, FcγRII and SIRPα are not homogeneously distributed at macrophage surfaces but are organized in discrete nanoclusters, with mean radius 71 ± 11 nm, 60 ± 6 nm and 48 ± 3 nm, respectively. Nanoclusters of FcγRI, but not FcγRII, are constitutively associated with nanoclusters of SIRPα, within 62 ± 5 nm, mediated by the actin cytoskeleton. Upon Fc receptor activation, Src-family kinase signaling leads to segregation of FcγRI and SIRPα nanoclusters to be 197 ± 3 nm apart. Co-ligation of SIRPα with CD47 abrogates nanocluster segregation. If the balance of signals favors activation, FcγRI nanoclusters reorganize into periodically-spaced concentric rings. Thus, a nanometer- and micron-scale reorganization of activating and inhibitory receptors occurs at the surface of human macrophages concurrent with signal integration.

Introduction

Macrophages play a key role in immune defenses by phagocytosis of pathogens and other harmful foreign particles. Phagocytosis can be initiated by the binding of Fcγ receptors (FcγRs) to the constant Fc domain of immunoglobulin (Ig) G molecules on opsonized particles. This interaction induces lateral clustering of FcγRs (Jaumouillé and Grinstein, 2011) and phosphorylation by Src-family kinases (SFKs) of the immunoreceptor tyrosine-based activation motif (ITAM) present in the receptor's cytosolic domain or on an associated common γ-chain (Ghazizadeh et al., 1994; Wang et al., 1994). Phosphorylation of the ITAM induces reorganization of the actin cytoskeleton, formation of a phagocytic synapse and engulfment of the target particle (Flannagan et al., 2012).

FcγRs are presumed to exist as monomers and be evenly distributed on the cell surface (Jaumouillé et al., 2014). Upon interaction with their ligand, FcγRs are thought to diffuse through the surface membrane to accumulate around a particle by a zipper-like mechanism (Griffin et al., 1975). Serial binding of Fc receptors to ligands extends a pseudopod along the particle, and integrins aid its progression and closure of the phagocytic cup (Freeman et al., 2016). Triggering of this process is dependent on the balance of signals from specific activating and inhibitory receptors.

SIRPα negatively regulates macrophage phagocytosis (Fujioka et al., 1996; Jiang et al., 1999; Okazawa et al., 2005; Oldenborg et al., 2001; Veillette et al., 1998) by interacting with CD47, essentially a 'marker of self' (Oldenborg et al., 2000). Ligation of the commonly expressed form of CD47 results in phosphorylation of the immunoreceptor tyrosine-based inhibition motif (ITIM) on the cytoplasmic tail of SIRPα, which leads to the recruitment of the tyrosine phosphatase SHP-1. This blocks phagocytosis, at least in part by preventing the accumulation of myosin-II A at the phagocytic synapse (Tsai and Discher, 2008).

Recently, super-resolution microscopy has established that many receptors are clustered at the plasma membrane on a nanometer-scale (Parajo-Garcia et al., 2014) and that the nanoscale organization of T cell, NK cell or B cell surfaces change when cells are activated (Klasener et al., 2014; Lillemeier et al., 2010; Mattila et al., 2013; Pageon et al., 2013). In macrophages, confocal fluorescence microscopy has established that both the inhibitory receptor SIRPα and the activating FcγRI accumulate at the phagocytic cup upon binding to their cognate ligands (Tsai and Discher, 2008; Yamauchi et al., 2012). Here, we used dual-color direct stochastic optical reconstruction microscopy (dSTORM) (Heilemann et al., 2008) to visualize the spatial organization of the activating FcγRs and the inhibitory receptor SIRPα with a lateral resolution of 25 nm on human macrophages. This revealed an unexpected nano- and micro-scale rearrangement of macrophage cell surface receptors concurrent with signal integration.

Results

FcγRI and SIRPα are arranged in discrete nanoclusters at macrophage surfaces

To determine the organization of the inhibitory receptor SIRPα and the high-affinity Fc receptor FcγRI at a nanometer-scale we employed the super-resolution microscopy technique dSTORM. For this, human monocyte-derived macrophages (hereafter referred to as primary macrophages; phenotyped in Fig. S1 A) were plated onto poly-L-lysine coated slides (PLL, non-activating condition) for 10 min, fixed and stained with directly labeled anti-SIRPα or anti-FcγRI mAbs (Fig. 1). dSTORM images, along with Ripley's K analysis (Ripley, 1977), of cells seeded under non-activating conditions revealed that both receptors are not randomly distributed but instead organized in discrete and spatially separated nanoclusters at the cell surface (Fig. 1 A and B, top row).

We next assessed the distribution of the receptors when cells were seeded onto glass slides coated with human IgG (hIgG), the ligand for FcγRs. This two-dimensional (2D) model of the phagocytic synapse creates a flattened focal plane amenable for dSTORM. Cells were plated for 10 min on slides coated with 10 µg/ml of hIgG, fixed and stained as before. Upon activation of FcγRs, both FcγRI and SIRPα were predominantly organized in specific nanoclusters (Fig. 1 A and B, bottom row).

To gain quantitative insight, we reconstituted the super-resolution images as probability density maps of the molecules based on univariate Getis and Franklin's local point pattern analysis (Getis and Franklin, 1987; Williamson et al., 2011). After thresholding, density maps were converted to binary maps in which regions containing dense localizations of the receptors appear white (referred to as nanoclusters, Fig. 1 A and B). Quantitative analysis revealed that SIRPα is constitutively arranged in nanoclusters with a mean area of 7,150 ± 980 nm^2 (Fig. 1 C), corresponding to a radius of 48 ± 3 nm (assuming nanoclusters are circular), and a mean density of 6.4 ± 1 nanoclusters/μm^2 (Fig. 1 D). These became smaller

(5,440 ± 1,095 nm^2, 42 ± 4 nm radius, Fig. 1 C) and less dense (3.9 ± 1 nanoclusters/μm^2, Fig. 1 D) after activation through FcγRI. In contrast, the proportion of localizations in nanoclusters (i.e. the number of localizations in nanoclusters divided by the total number of localizations) increased slightly (mean of 64 ± 6 % in non-activating conditions to 77 ± 7 % after activation, Fig. 1 E). FcγRI constitutively forms larger (mean area of 15,650 ± 5,030 nm^2, 71 ± 11 nm radius) and less dense (mean of 2.9 ± 0.3 nanoclusters/μm^2) nanoclusters than SIRPα, containing a higher proportion of localizations (mean of 74 ± 7 %). The size (14,610 ± 4,030 nm^2, 68 ± 9 nm radius) of FcγRI nanoclusters remained the same, while their density (2.5 ± 0.4 nanoclusters/μm^2) decreased upon stimulation with hIgG (Fig. 1 C and D), and the proportion of localizations in nanoclusters increased (82 ± 5 %, Fig. 1 E). Flow cytometry showed a small decrease of 8% and 19% in gMFI for SIRPα and FcγRI, respectively, after activation of cells with surface-immobilized hIgG for 10 min (Fig. S1 B and C) suggesting a small fraction of both receptors are internalized from the interface.

An alternative method of analysis to discriminate clustered from randomly distributed molecules is based on deliberate variation of labeling density combined with cluster analysis and is insensitive to artifacts generated by over-counting of blinking fluorophores (Baumgart et al., 2016). To apply this here, SIRPα and FcγRI were labeled with a range of concentrations (0.01 - 50 µg/ml) of directly labeled antibodies and imaged by dSTORM. For each image, the number of total localizations per μm^2, the relative area covered by the cluster masks (η), obtained from thresholded binary maps, and the average density of localizations within the clusters (ρ) were calculated. As Baumgart et al. (2016) discussed in detail, clustered and random distributions can be discriminated by plotting the normalized density ρ/ρ_0 (where ρ_0 is the intersection of the density curves with the *y*-axis) against η. For randomly distributed molecules, a horizontal line is observed, whereas for clustered receptors there is an increase in ρ/ρ_0. By this analysis, SIRPα and FcγRI are clustered at the surface of primary human macrophages as ρ/ρ_0 increases when the labeling concentration increases (Fig. 1 F and G). Altogether, these data show that the inhibitory receptor SIRPα

and the high-affinity Fc receptor FcγRI are organized in membrane nanoclusters at the surface of primary human macrophages before and after activation of FcγRs.

Nanoclusters of SIRPα and FcγRI are constitutively associated but segregate upon stimulation with hIgG

We next set out to use dual-color dSTORM to investigate the relationship between SIRPα and FcγRI nanoclusters. To validate our imaging and analysis, a positive control for colocalization was included in which the same protein, FcγRI, was stained with a primary anti-FcγRI mAb conjugated with AF488 followed by isotype-specific secondary antibody conjugated with an alternative fluorophore, AF647 (Fig. 2 A, bottom row).

To examine the organization of SIRPα and FcγRI nanoclusters, cells were plated under non-activating conditions for 10 min before being fixed and stained with anti-FcγRI-AF488 and anti-SIRPα-AF647 mAbs. Dual-color dSTORM revealed that SIRPα nanoclusters are constitutively associated with FcγRI nanoclusters at the surface of primary human macrophages (Fig. 2 A, top row). The degree of colocalization between the two receptors was addressed by subjecting SIRPα and FcγRI localization lists to coordinate-based colocalization (CBC) analysis (Malkusch et al., 2012) which assigns a correlation coefficient to each single localization of each protein within a certain radial distance, ranging from -1 (perfectly segregated) through 0 (uncorrelated distributions) up to +1 (perfectly colocalized).

CBC analysis showed that, in non-activated cells, a large proportion of SIRPα is associated with FcγRI within a search radius of 50 nm, as demonstrated by the histogram distribution of the colocalization parameter being distributed towards +1 (50 % of localizations are between 0 and 1, Fig. 2 B). The search radius of 50 nm was chosen based on the mean radius of SIRPα nanoclusters in non-activating conditions. Corroborating this, the mean nearest-neighbor distance (NND) of paired single-molecule localizations was 42 ± 9 nm (Fig. 2 C). A proportion of SIRPα (36 ± 6 %) and FcγRI (26 ± 7%) molecules are not localized within

nanoclusters (Fig. 1 E), which could lower the degree of colocalization in CBC analysis. To test directly whether or not nanoclusters associate, we measured the NND between the centroids of nanoclusters of the two receptors. The centroid NND between SIRPα and FcγRI nanoclusters has a mode of 62 ± 5 nm (Fig. 2 D).

To test whether or not such close association between SIRPα and FcγRI nanoclusters occurs by chance, simply as an outcome of the density of nanoclusters at the cell surface, we next analyzed simulated images in which the centroid positions of SIRPα nanoclusters were randomized within the cell area. The mode of the centroid NND was 122 ± 2 nm for these simulated images, compared to 62 ± 5 nm in experimental data (Fig. 2 D). This confirms a specific association between SIRPα and FcγRI nanoclusters in non-activated macrophages.

Upon activation of FcγRI, the two receptors segregated from each other (Fig. 2 A, middle row), as indicated by an increase in the proportion of SIRPα molecules with negative correlation coefficients (towards -1, Fig. 2 B) and a significant increase in the NND between individual localizations of both receptors (to a mean of 101 ± 24 nm, Fig. 2 C). Moreover, the centroid NND between SIRPα and FcγRI nanoclusters increased (Fig. 2 D). Indeed, the mode for the centroid NND between SIRPα and FcγRI nanoclusters, upon FcγRI ligation, was 197 ± 3 nm and 207 ± 3 nm for experimental and simulated data, in which the positions of SIRPα nanoclusters were randomized, respectively. In contrast, CBC analysis of the positive control-stained cells showed a very high degree of colocalization (Fig. 2 B) with a mean NND of paired single-molecule localizations of 15 ± 4 nm (Fig. 2 C) and a mode for the centroid NN distances between nanoclusters of 28 ± 1 nm (Fig. 2 D). After 30 min of stimulation, there was no significant difference in any parameter describing the organization of SIRPα or FcγRI nanoclusters (Fig. S1 B and C, Fig. S2), showing that segregation of these nanoclusters persists. Thus, upon ligation, SIRPα and FcγRI nanoclusters are no longer associated and become distributed independently (Fig. 2 D).

Nanoclusters of SIRPα and FcγRII are constitutively segregated

To test if the association between SIRPα and FcγRI nanoclusters is specific, we next studied the relationship between SIRPα and the low-affinity activating Fc receptor FcγRII (CD32). Similar to SIRPα and FcγRI, FcγRII also assembles in discrete nanoclusters at the surface of primary human macrophages, both constitutively and upon activation with hIgG (Fig. 3 A and B). Quantitative analysis showed that, in non-activated cells, at 10 min, FcγRII nanoclusters have a mean area of 11,400 ± 2,400 nm^2 (corresponding to a mean radius of 60 ± 6 nm), a mean density of 4.4 ± 1 nanoclusters/μm^2, and a mean percentage of localizations in nanoclusters of 76 ± 4 % (Fig. 3 C-E). These values remained largely unchanged after activation with hIgG for 10 min (Fig. 3 C-E). However, after 30 min of activation, FcγRII nanoclusters became larger (mean area of 16,900 ± 6,540 nm^2, mean radius of 73 ± 13 nm, Fig. 3 C) and less dense (mean density of 2.7 ± 1 nanoclusters/μm^2, Fig. 3 D). Flow cytometry showed no significant change in FcγRII expression levels after activation (Fig. S1 D).

In contrast to FcγRI, FcγRII is not associated with SIRPα, in non-activated cells or upon activation (Fig. 4 A). This was confirmed by CBC analysis (distribution of the CBC histograms towards negative correlation coefficients and mean NND of paired single-localizations all > 50 nm; Fig. 4 B and C) and by the centroid NND (with a mode of ~ 140 nm in all conditions; Fig. 4 D). Altogether, these observations indicate that under non-activating conditions, SIRPα is associated at the nanometer-scale with the high-affinity Fc receptor FcγRI, but not with the low-affinity Fc receptor FcγRII, and upon activation, SIRPα and FcγRI nanoclusters segregate.

FcγRI and FcγRII reorganize into concentric rings upon activation

When plated onto IgG-coated slides, macrophages spread to a uniform radial morphology with multiple pseudopod extensions (Cannon and Swanson, 1992; Heiple et al., 1990). Here,

TIRF microscopy of primary human macrophages was used to examine the location of FcγRI and FcγRII within the morphology of activated cells (Fig. 5 A). Unexpectedly, both types of FcγR were found to reorganize into concentric rings at the surface of macrophages stimulated by slides coated with hIgG. Redistribution of the high-affinity Fc receptor, FcγRI, into concentric rings was detected as early as after 10 min of incubation, whereas that of the low-affinity Fc receptor, FcγRII, was visible after 30 min (Fig. 5 A). In contrast, when plated under non-activating conditions, macrophages spread asymmetrically and FcγRs did not reorganize into concentric rings at any time of incubation (Fig. 5 A).

Live cell TIRF microscopy was used to visualize formation of the ring structures. Cells were labeled in suspension with a directly conjugated non-blocking anti-FcγRI mAb and imaged as they landed onto non-activating PLL-coated (Video 1) or activating hIgG-coated slides (Video 2). In non-activating conditions cell shape was irregular and FcγRI nanoclusters remained homogeneously distributed at the cell surface. On slides coated with hIgG, cells spread rapidly and uniformly, and the formation of the rings was concurrent with cell spreading. Rings of FcγRI periodically assembled at the leading edge of the cell, until spreading stopped.

Formation of the rings could result solely from the redistribution of the receptors already present at the synapse, or in addition, from the recruitment of proteins from other parts of the cell to the phagocytic synapse. To investigate this, we acquired confocal images of cells allowed to spread under non-activating (Fig. S3 A) or hIgG-activating (Fig. S3 B) conditions for 10 min before fixation and staining for FcγRI. 3D confocal image reconstruction indicated that FcγRI is recruited to the activating interface (Fig. S3 B, Video 3), while it remains homogeneously distributed throughout the cell surface in non-activating conditions (Fig. S3 A, Video 4). Thus, Fc receptors are recruited into the interface from around the cell surface.

To determine whether or not rings of the two FcγRs colocalized, cells were seeded onto non-activating PLL- or activating hIgG-coated slides for 10 or 30 min, fixed and stained with anti-FcγRI-AF488 and anti-FcγRII-AF647. Dual-color dSTORM revealed that FcγRI and FcγRII segregated at the nanometer-scale in non-activating conditions, as well as after 10 min of activation by hIgG (Fig. 5 B). CBC analysis (Fig. 5 C) and the mean NND of paired single-molecule localizations (Fig. 5 D) confirmed that FcγRI and FcγRII are segregated in non-activated cells, or cells activated for 10 min. The mode of NND between nanoclusters of the two receptors was greater than 110 nm in each of these conditions (Fig. 5 E). However, after 30 min of activation, when both receptors form concentric rings, FcγRI and FcγRII were colocalized (Fig. 5 B), evidenced by the CBC histogram distribution towards +1 (Fig. 5 C), the mean NND between localizations of 32 ± 16 nm (Fig. 5 D), and the mode of NND between nanoclusters of 61 ± 10 nm (Fig. 5 E). Thus, the assembly of rings of Fc receptor brings FcγRI and FcγRII together on a nanometer-scale.

To establish whether or not ligation of Fc receptors or cellular activation in general causes segregation of FcγRI from SIRPα, and the assembly of rings of FcγRs, the effect of two different hIgG isotypes, hIgG1 and hIgG2, were compared. The high-affinity Fc receptor FcγRI can only be activated by hIgG1 and not hIgG2 while the low-affinity Fc receptor FcγRII can be activated by both isotypes (Bruhns et al., 2009). If cellular activation in general is responsible for these rearrangements then FcγRI would segregate from SIRPα and form concentric rings on hIgG2-coated surfaces that activate macrophages through other FcγRs but not FcγRI. In contrast, if these events were a consequence of specific ligation then both segregation between FcγRI and SIRPα and reorganization of FcγRI into rings would only be observed when the Fc receptor is ligated by hIgG1.

To test this, cells were plated onto hIgG1- or hIgG2-coated slides for 10 or 30 min, stained with anti-FcγRI-AF488 and anti-SIRPα-AF647 mAbs and imaged. On hIgG1-coated slides, SIRPα and FcγRI nanoclusters were segregated and FcγRI reorganized into concentric rings

(Fig. 6 A and B, top row), resembling the results obtained with total hIgG. In contrast, when cells were plated onto hIgG2-coated slides, which activates cells via FcγRII, the FcγRI and SIRPα remained associated and FcγRI did not reorganize into concentric rings (Fig. 6 A and B, bottom row). CBC analysis showed a shift in the CBC histogram towards -1 (Fig. 6 C) and a mean NND between localizations of 140 ± 31 nm (Fig. 6 D) on hIgG1, while the CBC histogram is shifted towards +1 upon stimulation with hIgG2 (Fig. 6 C) and the mean NND of paired single-molecule localizations was 61 ± 26 nm (Fig. 6 D). The mode of the centroid NND between nanoclusters was 181 ± 3 nm on hIgG1 and 66 ± 5 nm on hIgG2 (Fig. 6 E). These results were not time-dependent as the analysis was similar for 10 or 30 min of incubation (Fig. 6 B-E).

In contrast to FcγRI, FcγRII could reorganize into concentric rings after interacting with either hIgG1 or hIgG2 (Fig. S4 B). Reorganization of FcγRII occurred only after 30 min of incubation, not after 10 min (Fig. S4), as consistent with stimulation with hIgG (Fig. 5 A) and, when plated onto hIgG1-coated slides, FcγRII colocalized with FcγRI (Fig. S4 B). Thus, these data establish that the reorganization of FcγRI and FcγRII into a specific pattern of concentric rings occurs as a consequence of receptor ligation and not of cellular activation in general.

The nanoscale organization of macrophage surfaces alters upon activation by membrane-bound IgG.

To determine whether or not similar changes occur to the macrophage cell surface upon activation by mobile ligands, macrophages were seeded onto planar glass-supported lipid bilayers (SLB) enriched with laterally mobile hIgG. After 10 min incubation, cells were fixed, stained with anti-FcγRI-AF488 and anti-SIRPα-AF647. For cells plated onto control SLB, lacking hIgG, macrophage spreading was irregular and FcγRI nanoclusters were distributed across the cell surface (Fig. 7 A). In contrast, when cells were plated onto hIgG presented by

SLB, macrophages spread to a uniform radial morphology and FcγRI reorganized into concentric rings around a dense central accumulation (Fig. 7 A).

Quantitative analysis confirmed that SIRPα and FcγRI were organized in discrete nanoclusters on the surface of macrophages interacting with SLB (Fig. 7 B-E), with characteristics similar to that for macrophages interacting with immobilized ligands on glass slides (Fig. 7C-E). SIRPα assembled in slightly smaller nanoclusters (mean area of 5,800 ± 630 nm^2, 43 ± 2 nm radius, Fig. 7 C) and nanoclusters were less abundant (mean of 4.6 ± 1.1 nanoclusters/μm^2, Fig. 7 D) in comparison to cells interacting with glass slides. However, both the size and density of SIRPα nanoclusters decreased on hIgG-presenting SLB (Fig. 7 C and D) as seen for immobilized hIgG. Most importantly, on control SLB, SIRPα and FcγRI nanoclusters were localized in close proximity (distribution of the CBC histograms towards positive correlation coefficients, mean NND of paired single-localizations of 32 ± 12 nm, and a mode for the centroid NND of 23 ± 13 nm, Fig. 7 F-H) but segregated on hIgG-presenting SLB (distribution of the CBC histograms towards negative correlation coefficients, mean NND of paired single-localizations of 95 ± 32 nm, and a mode for the centroid NND of 163 ± 3 nm, Fig. 7 F-H). Thus, nanoclusters of activating FcγRI segregate from inhibitory SIRPα and reorganize into concentric rings in a model of frustrated phagocytosis in which the activating ligand is embedded in lipid bilayers and is mobile.

Ligation of SIRPα impairs the reorganization of surface FcγRI

We next asked whether the inhibitory signal from SIRPα could affect the micrometer- and nanometer-scale organization of these receptors. For this, cells were plated for 10 min onto slides coated with recombinant human CD47 protein (hCD47), to ligate SIRPα, and hIgG to activate FcγRs, separately or in combination. Incubation of macrophages with hIgG led to release of M-CSF, measured by ELISA, which was reduced to basal levels in the presence of hCD47 (Fig. 8 A), confirming that hCD47 acted as a potent inhibitor of Fc receptor signals. In addition, upon co-ligation of SIRPα and Fc receptors, cells spread to an irregular shape

(Fig. 8 B) and did not show the circular morphology characteristic of Fc receptor activation (Cannon and Swanson, 1992; Heiple et al., 1990). As before, stimulation with hIgG alone resulted in segregation of FcγRI and SIRPα (Fig. 8 D-F). However, segregation of these receptors caused by ligation of FcγRI, could be abrogated by the simultaneous ligation of SIRPα with hCD47 (Fig. 8 C, bottom row). CBC histograms did not reflect a strong level of inhibition by SIRPα (on account of the 50 nm search radius; Fig. 8 D), but the mean NND of paired single-molecule localizations (79 ± 18 nm, Fig. 8 E) and the mode of the centroid NND (89 ± 2 nm, Fig. 8 F) were significantly decreased upon co-ligation of inhibitory receptors (compared to ligation of Fc receptors alone, Fig. 8 E and F). In addition, FcγRI did not reorganize into concentric rings when SIRPα was co-ligated with the Fc receptors (Fig. 8 B). These results were reproduced after 30 min incubation time, establishing that co-ligation of SIRPα does not merely delay the reorganization of cell surface nanoclusters (Fig. S5).

To further address if the nanoscale organization of the receptors is important for signal integration, we imaged FcγRI with SHP-1, the phosphatase recruited by SIRPα after activation with CD47, phosphorylated on tyrosine 536 (pSHP-1^{Y536}), as a marker of phosphatase activity. Cells were plated for 5 min onto slides again coated with hCD47, to ligate SIRPα, and hIgG to activate FcγRs separately or in combination. Since SIRPα and FcγRI remain associated after ligation of SIRPα, recruitment of SHP-1 by the inhibitory receptor would bring the phosphatase to the close proximity of FcγRI. As such, ligation of SIRPα with CD47 resulted in the colocalization between pSHP-1^{Y536} and FcγRI nanoclusters (Fig. 8 G-I). Importantly, co-ligation of FcγRI and SIRPα also led to the colocalization between the activating receptor and pSHP-1^{Y536}. The CBC histrogram was shifted towards +1 (Fig. 8 G), and both the mean NND of paired single-molecule localizations (62 ± 16 nm, Fig. 8 H) and the mode of the centroid NND (56 ± 2 nm, Fig. 8 I) were similar to the when SIRPα was ligated alone.

Overall, these data establish that signal integration between positive and negative signaling receptors impacts the nanoscale organization of the macrophage cell surface; colocalization of SIRPα and FcγRI nanoclusters correlates with cellular inhibition while segregation of these nanoclusters correlates with activation.

The actin cytoskeleton controls the proximity of SIRPα and FcγRI nanoclusters

One way in which proteins are organized at the cell surface is through interactions with the actin cytoskeleton (Lagrue et al., 2013, Mattila et al., 2013). To address the role of the cytoskeleton in the organization of SIRPα and FcγRI, macrophages were treated with pharmacological agents that interfere with the actin cytoskeleton. Treatment with latrunculin A (Lat A), which disrupts the organization of filamentous actin by binding to, and sequestering, monomeric actin, induced the segregation of FcγRI and SIRPα in non-activated cells (Fig. 9 A-D). This was indicated by the distribution of CBC histograms towards negative correlation coefficients (Fig. 9 B) and an increase in the NND of paired single-localizations (mean of 108 ± 17 nm; Fig. 9 C). In addition, the centroid NND between SIRPα and FcγRI nanoclusters increased (mode of 103 ± 3 nm; Fig. 9 D). Similarly, treatment with Jasplakinolide (Jasp), which stabilizes actin filaments, induced a small extent of segregation of nanoclusters in non-activated conditions that became more pronounced upon stimulation with hIgG (Fig. 9 A-D). In both cases, the reorganization of FcγRI nanoclusters into concentric rings after stimulation was abolished (Fig. 9 A). In contrast, drugs which inhibit the activity of formins (SMIFH2; 1-(3-Bromophenyl)-5-(2-furanylmethylene)dihydro-2-thioxo-4,6(1H,5H)-pyrimidinedione) or myosin II (blebbistatin) had little, if any, effect on the segregation of SIRPα and FcγRI nanoclusters (Fig. 9 A-D).

Assembly of the ring-shaped organization of FcγRI, however, was abolished by the inhibition of formins and not by inhibition of myosin II (Fig. 9 A), indicating that formins are important for this process. This also establishes that the assembly of Fc receptor into ring-shaped structures can be uncoupled from the segregation of SIRPα and FcγRI nanoclusters.

Inhibition of myosin II by blebbistatin prevented the internalization of SIRPα at the interface to some extent (Fig. 9 E-G). Both the area (Fig. 9 E) and the density (Fig. 9 F) of SIRPα nanoclusters after hIgG-stimulation was not as decreased as in DMSO-treated cells, suggesting that this process requires the activity of myosin II and that this too is independent from the segregation of SIRPα and FcγRI nanoclusters triggered upon activation. Together, these data establish that the constitutive association of FcγRI and SIRPα nanoclusters requires the actin cytoskeleton and that the mechanism underlying the segregation of receptors and the reorganization of FcγRI into concentric rings is dependent on the actin cytoskeleton and formins but not myosin II.

Segregation of FcγRI from SIRPα and reorganization of FcγRI into concentric rings is dependent on Src-family kinase signaling

To better understand the mechanism of SIRPα and FcγRI segregation, and the reorganization of the Fcγ receptor into concentric rings, we next set out to dissect the signaling pathways involved, using drugs known to target specific components of the phagocytic machinery. The effectiveness of PP2 (a SFK inhibitor), piceatannol (a Syk inhibitor) and wortmannin (a PI3K inhibitor) was verified by immunoblotting with an antibody for phosphorylated AKT, a downstream target of both SFK and PI3K signaling (Fig. 10 A).

Inhibition of Syk or PI3K had no effect on the segregation of SIRPα and FcγRI, or on the reorganization of FcγRI into concentric rings, upon activation of cells with hIgG (Fig. 10 B). Both CBC analysis and centroid NND analysis showed equivalent segregation of receptors in control-treated cells or cells treated with either of the two drugs (Fig. 10 C-E). In contrast, when SFKs were inhibited, SIRPα and FcγRI remained colocalized after stimulation of cells with hIgG (Fig. 10 B and C) with a mean NND between localizations (62 ± 22 nm) and a mode for the centroid NND (71 ± 1 nm) similar to DMSO-treated control cells in non-activating conditions (mean NND between localizations of 62 ± 23 nm and mode of the centroid NND of 52 ± 3 nm, Fig. 10 D and E). In addition, the assembly of Fc receptor rings

was abrogated by PP2 (Fig. 10 B). Thus, membrane proximal signaling by SFKs is important for the nanometer- and micrometer-scale reorganization of the macrophage cell surface.

Discussion

It is well established that immune cell receptors and ligands are organized into micrometer- and submicron-scale domains at cell surfaces and immune synapses (Bunnell et al., 2002; Davis and Dustin, 2004; Harwood and Batista, 2008; Orange, 2008). Recently however, the development of super-resolution microscopy techniques has extended this view by providing evidence that many proteins are organized in plasma membrane domains on a nanometer-scale (Parajo-Garcia et al., 2014).

A previous study indicated that FcγRII is constitutively expressed as monomers and upon ligation, increases its lateral mobility and clustering (Jaumouillé et al., 2014). Here, exploiting recent developments in super-resolution microscopy, we revise this model of the macrophage cell surface by establishing that the activating receptors FcγRI and FcγRII, and the inhibitory receptor to prevent phagocytosis of self, SIRPα, are constitutively organized in discrete nanometer-scale domains at the surface of primary human macrophages with SIRPα forming smaller but more numerous nanoclusters than the Fc receptors.

In non-activated cells, nanoclusters of FcγRI, but not FcγRII, are associated with nanoclusters of SIRPα. Ligation of SIRPα recruits the phosphatase SHP-1 which likely acts locally. Thus, the proximity between FcγRI and SIRPα is likely to be important for SIRPα-mediated inhibition of the Fc receptor signaling. Disruption of filamentous actin organization induced the segregation between SIRPα and FcγRI even in non-activating conditions. This suggests that the constitutive association between the two receptors is regulated to at least some extent by the actin cytoskeleton.

For T cells and B cells, activating signals are concurrent with the segregation of phosphatase activity from kinase activity (Chang et al., 2016). Here, stimulation with hIgG induced segregation of FcγRI and SIRPα nanoclusters. This likely hinders the ability of

SIRPα signaling to suppress FcγRI signaling and thereby provides a positive feedback to amplify or sustain cellular activation. In contrast, co-ligation of SIRPα with CD47 abrogated the segregation of SIRPα and FcγRI nanoclusters, and promoted the recruitment of pSHP-1^{Y536} to the proximity of FcγRI nanoclusters, thereby helping prevent cellular activation. Previous imaging has not detected these nanoscale rearrangements at the cell surface because they could not be resolved by standard light microscopy.

Interaction with IgG also induced the reorganization of FcγRs at a micrometer-scale. After cross-linking, FcγRs were recruited to the frustrated phagocytic synapse, where they formed periodically spaced concentric rings. Live imaging of FcγRI showed that the reorganization of the receptor into concentric rings is coincident with cell spreading on activating surfaces. An expanding integrin wave is known to extend beyond the perimeter of the receptor-ligand engagement zone and facilitate the zippering of FcγRs onto the target (Freeman et al., 2016). It is possible that this actin-tethered integrin wave may play a role in positioning FcγRs in concentric rings, such that the rings of Fc receptor mark out the spaced teeth of a phagocytic zipper.

Mechanistically, the reorganization of FcγRI into concentric rings, as well as the segregation of SIRPα and FcγRI nanoclusters, is dependent on the actin cytoskeleton. Assembly of the ring-shaped structure of FcγRI is also dependent on formins, but independent of myosin II activity. In contrast, myosin II activity is important for the internalization of SIRPα triggered by FcγRI ligation. Moreover, inhibition of SFKs, which are essential for an efficient phagocytic response, prevented these rearrangements of the macrophage cell surface. Thus, impairing the actin cytoskeleton or blocking the phagocytic signal, either by inhibiting the activating signal with pharmacological drugs or by ligating the inhibitory receptor, hindered both the segregation between FcγRI and SIRPα and the reorganization of FcγRI into concentric rings, pointing to these behaviors being an important feature of the phagocytic response.

In summary, the high-affinity Fc receptor FcγRI is kept in close proximity to the inhibitory receptor SIRPα by the actin cytoskeleton in non-activated macrophages. But upon ligation of FcγRI, nanoclusters of FcγRI segregate from nanoclusters of SIRPα. This occurs concurrently with a micrometer-scale reorganization of activating Fc receptors into concentric rings, dependent on SFK signaling. Co-ligation of SIRPα abrogates this segregation of nanoclusters, promotes the recruitment of pSHP-1^{Y536} to the proximity of FcγRI, and prevents the assembly of Fc receptor rings. Altogether, these data reveal an unexpected nanometer- and micrometer-scale rearrangement of the macrophage cell surface concurrent with signal integration.

Material and Methods

Generation of macrophages

Peripheral blood from healthy donors was acquired from the NHS blood service under ethics license REC 05/Q0401/108 (University of Manchester). Peripheral blood mononuclear cells (PBMCs) were isolated by density gradient centrifugation (Ficoll-Paque Plus; Amersham Pharmacia Biotech). Human monocyte-derived macrophages were derived as described previously (Davies and Gordon, 2005). In brief, $CD14^+$ cells were isolated by positive selection from PBMCs using magnetic beads (CD14 MicroBeads; Miltenyi Biotec) and cultured at 10^6 cells/ml in serum-free media (X-Vivo 10, Lonza) supplemented with 1% human serum (Sigma). After 24 hours, monocytes were washed with phosphate-buffered saline (PBS, Sigma) to remove non-adherent cells and cultured in X-Vivo media with 1% human serum. After 3 days of incubation, adherent cells were washed with PBS and cultured in standard DMEM-based media (Sigma) supplemented with 10% fetal bovine serum (FBS, Invitrogen), 1% penicillin and streptomycin (Gibco), 1% L-glutamine (Gibco) and 1% HEPES (Sigma) for six days to generate monocyte-derived macrophages, phenotyped to be $CD14^+$, $CD11a^+$, $CD3^-$, $CD56^-$ and $CD19^-$. Cells were washed with PBS and media was replaced every three days.

Flow cytometry

To assess surface expression of SIRPα and FcγRI cells were washed and blocked with 2% FBS/PBS for 30 min at 4ºC, and stained with Zombie Aqua™ viability dye (Biolegend), anti-CD14 mAb (clone 61D3, eBiosciences) conjugated with FITC and anti-SIRPα mAb (clone SE5A5, Biolegend) or anti-FcγRI (clone 10.1, Biolegend), respectively, conjugated with APC or isotype-matched control mAbs (mouse IgG1 isotype control, clone MOPC-21, Biolegend, conjugated with FITC or APC) for 30 min at 4ºC. To assess surface expression of FcγRII cells were washed and blocked as before, stained with Zombie Aqua™ viability dye, anti-CD14 mAb (clone 61D3, eBiosciences) conjugated with APC anti-FcγRII mAb (clone

FLI8.26, BD Biosciences) or isotype-matched control mAb (mouse IgG2b isotype control, clone MPC-11, BD Biosciences) for 30 min at 4ºC, washed twice with 2% FBS/PBS, and incubated with fluorescently labeled anti-mouse IgG2b secondary Ab (Invitrogen) conjugated with AF488 for 30 min at 4ºC. Finally, cells were washed in 2% FBS/PBS, fixed in 2% PFA/PBS, assessed by BD FACS Canto II flow cytometer (BD Biosciences) and analyzed (FlowJo_V10 software).

For phenotyping monocyte-derived macrophages were stained with anti-CD14 mAb (clone 61D3, eBiosciences), anti-CD11a mAb (clone HI111, BD Biosciences), anti-CD3 mAb (clone UCHT1, Biolegend), anti-CD56 mAb (clone HCD56, Biolegend), and anti-CD19 mAb (clone HIB19, Biolegend), or isotype-matched control mAb [mouse IgG1 isotype control, clone MOPC-21, conjugated with APC or PE (Biolegend), or FITC (BD Biosciences)]. Anti-CD14 and anti-CD11a mAbs are conjugated with APC and FITC, respectively, while anti-CD3, anti-CD56 and anti-CD19 mAbs are conjugated with PE.

Enzyme-linked immunosorbent assay (ELISA)

Primary monocyte-derived macrophages were incubated on chambered glass coverslips coated with PLL, human CD47-Fc or human IgG, as indicated, at 37ºC for 24 h. Cell supernatants were recovered and centrifuged at 350 g for 10 min at RT to remove cell debris. M-CSF production was quantified in the supernatants by sandwich ELISA (DuoSet® ELISA, R&D Systems), according to manufacturer's instructions. The plates were developed with TMB ELISA substrate (Sigma) and the reaction was stopped with 1 N H_2SO_4. Absorbance was measured at 450 nm using a 570 nm reference line.

Drug treatments

Primary human macrophages were pre-treated with 10 μM of either the Src-family kinase inhibitor PP2 (Sigma),or the myosin II inhibitor Blebbistatin (Sigma), with 100 μM of the Syk kinase inhibitor Piceatannol (Sigma), or with 0.5 μM Jasplakinolide (Sigma) for 30 min, or

with 1 μM of either Latranculin A (Calbiochem), or the PI3K inhibitor Wortmannin (Sigma), or with 10 μM of the formin inhibitor SMIFH2 (Sigma) for 10 min, in PBS at 37°C. As a control, cells were incubated with DMSO. After incubation, cells were resuspended in culture medium and plated onto coverslips under non-activating or activating conditions for 10 min, as indicated, before being fixed and stained for imaging.

Immunoblotting

Primary human macrophages were pre-treated as described above and plated onto PLL- or hIgG-coated slides for 10 min at 37°C. After incubation, adherent cells were rinsed twice in ice-cold PBS and disrupted with ice-cold lysis buffer containing 10 mM Tris-HCl pH 7.4, 100 mM NaCl, 1mM NaF, 1 mM orthovanadate, 0.5% NP-40 and protease inhibitors (Cφmplete™ EDTA-free protease inhibitors, Roche). Lysates were cleared by centrifugation and reduced in Laemmli's buffer, resolved by SDS-PAGE, transferred to nitrocellulose membrane and immunoblotted with anti-phospho-AKT Ser 473 (clone 193H12, Cell Signaling) and anti-actin (Sigma) antibodies.

Sample preparation for imaging

Chambered glass coverslips (#1.5 Lab-Tek II, Nunc) were coated with 0.01% poly-L-lysine (PLL, Sigma) and used for imaging of unstimulated cells or coated with 10 μg/ml of human CD47-Fc (R&D Systems), 10 μg/ml of human IgG, 10 μg/ml human IgG1 or 10 μg/ml human IgG2 (freshly resuspended in 150 mM NaCl, all from Sigma) in PBS, overnight at 4ºC, as indicated, for stimulation of cells. Cells were allowed to settle on the slides for 5, 10 or 30 min at 37ºC, fixed with 4% PFA/PBS for 15 min at RT and washed three times in PBS. In other experiments, we confirmed that similar results were obtained when cells were fixed with 4% PFA/PBS for 1 hour or with 4% PFA/0.2% glutaraldehyde for 30 mins. Samples were blocked in 3% BSA/PBS for 1 hour at RT followed by incubation with the appropriate fluorescently labeled mAbs, diluted in 3% BSA/PBS for 1 hour at RT. Whenever intracellular staining was required cells were first permeabilized and blocked with 3% BSA/0.2% Triton X-

100/PBS at RT for 1 h before incubation with the antibody. Samples were then washed, post-fixed with 4% PFA/PBS for 5 min at RT and imaged. Primary monoclonal antibodies used for microscopy were: anti-SIRPα (clone 4C7, AbD Serotec) conjugated in house with AF647 (Invitrogen), anti-FcγRI-AF488 (clone 10.1, Biolegend), anti-FcγRII (clone FLI8.26, BD Biosciences) conjugated in house with Atto488 (Invitrogen) or AF647, and anti-PTPN6(Tyr536)-AF647 (Bioss). All in house labeled antibodies had 6-7 dyes/antibody.

Supported lipid bilayers

Preparation of liposomes and planar bilayer formation are described in detail elsewhere (Dustin et al., 2007). Briefly, for coupling of streptavidin-conjugated hIgG, prepared using a Streptavidin Conjugation Kit (Abcam) according to the manufacturer's instructions, 2 mol% DOPE-cap-Biotin in DOPC were deposited onto clean glass coverslip of the flow chamber (sticky-Slide VI 0.4, Ibidi). As a control, planar bilayers were coupled with streptavidin-AF647 (Molecular Probes). Lipid droplets were trapped by overlaying glass coverslips cleaned using peroxidated H_2SO_4. Chambers were flooded with HEPES buffered saline supplemented with 0.1% bovine serum albumin (BSA), and flushed to remove excess liposomes, leaving deposited DOPC bilayers containing 2 mol% DOPE-cap-Biotin. Bilayers were uniformly fluid as measured by photobleaching/recovery. Following blocking for 30 min with HBS supplemented with 2% BSA, fluorescently labeled (or unlabeled) hIgG was incubated on bilayers for 30 min. Protein concentrations required to achieve desired densities on bilayers were calculated from calibration curves constructed from flow-cytometric measurements of bilayer-associated fluorescence of attached proteins on bilayers form on glass beads, compared to reference beads containing known numbers of the appropriate fluorophore (Bangs Laboratories). All lipids were purchased from Avanti Polar Lipids. Cells were allowed to settle and form contacts with the bilayer for 10 min before being fixed with 4% PFA for 15 min, labeled and imaged by dSTORM.

Confocal imaging

Confocal imaging (Leica TCS SP8) was carried out using a 100x 1.4 N.A. oil immersion objective. Cells were plated onto PLL- or hIgG-coated slides for 10 min, fixed and stained with NucBlue® Live Cell Stain (Invitrogen), membrane dye DiD (Invitrogen) and anti-FcγRI-AF488 mAb (clone 10.1, Biolegend). Images were taken with a frame rate of 600 Hz and 250 nm *z*-stepping. ImageJ (National Institutes of Health) was used for 3D rendering.

TIRF and live cell imaging

TIRF and live cell imaging (Nikon N-STORM) were performed using a 100x 1.49 N.A. oil immersion objective. For TIRF imaging, cells were plated onto PLL- or hIgG-coated slides for 10 or 30 min, fixed and stained with anti-FcγRI-AF488 (clone 10.1, Biolegend) or anti-FcγRII (clone FLI8.26, BD Biosciences) conjugated in house with Atto488 (Invitrogen) as described previously. For live cell imaging, cells were stained with anti-FcγRI-AF488 mAb as previously described for FACS experiments and imaged immediately as they landed onto PLL- or hIgG-coated slides. The emitted fluorescence was collected by the objective onto an electron-multiplying charge-coupled device (EM-CCD) camera (Andor IXON Ultra 897, Andor Technology). The frame rates used in the experiments were 100 (for PLL) or 200 (for hIgG) ms per frame for a maximum of 10 minutes. A focus lock system was used to keep the sample in focal plane.

dSTORM imaging

dSTORM imaging (Leica SR GSD) was carried out using a 160x 1.43 N.A. oil immersion objective in TIRF mode. Dual-color dSTORM imaging was performed with primary antibodies directly conjugated with AF647 and AF488 acquired in sequential manner. Firstly, 642 nm laser light was used for exciting the AF647 dye and switching it to the dark state. Secondly, 488 nm laser light was used for exciting the AF488 dye and switching it to the dark state. An additional 405 nm laser light was used for reactivating the AF647 and AF488 fluorescence. The emitted light from both dyes was collected by the same objective and imaged onto the EM-CCD camera at a frame rate of 10 ms per frame. A maximum of 5000 frames per

condition were acquired. For each receptor the specificity of the labeling was confirmed by staining cells with isotype-matched control antibodies (Fig. S3). These controls showed a negligible level of nonspecific binding (no more than 3 % of the total number of localizations per cell).

dSTORM data analysis

Since dual-color dSTORM imaging is performed in sequential mode by using two different optical detection paths (dichroic and emission filters are different), an image registration is required in order to generate the final two-color dSTORM image (Balint et al., 2013; Bates et al., 2012). Therefore, fiducial markers (TetraSpek Fluorescent Microspheres, Invitrogen) of 100 nm, which were visible in both 488 nm and 647 nm channels, were used to align the 488 nm channel to 647 nm channel. The images of the beads in both channels were used to calculate a polynomial transformation function that maps the 488 nm channel onto the 647 nm channel, using the MultiStackReg plug-in of ImageJ to account for differences in magnification and rotation, for example. The transformation was applied to each frame of the 488 nm channel. dSTORM images were analysed and rendered as previously described (Bates et al., 2007; Huang et al., 2008) using custom written software (Insight3, kindly provided by Prof. Bo Huang, University of California, San Francisco). Briefly, peaks in single molecule images were identified based on a threshold and fit to a simple Gaussian to determine the *x* and *y* positions. Only localizations with photon count higher than 400 photons were included and localizations that appeared within one pixel in five consecutive frames were merged together and fitted as one localization. The final images were rendered by representing the *x* and *y* positions of the localizations as a Gaussian with a width that corresponds to the determined localization precision. Sample drift during acquisition was calculated and subtracted by reconstructing dSTORM images from subsets of frames (500 frames) and correlating these images to a reference frame (the initial time segment).

Quantitative cluster analysis was based on Ripley´s *K* function (Ripley, 1977) and univariate Getis and Franklin´s local point pattern analysis (Getis and Franklin, 1987; Perry, 2004). The *x* and *y* coordinate list of localizations was used and multiple regions of 5 x 5 µm were selected for each cell giving the median value per cell. Spatial pattern analysis using Ripley´s *K* function was performed with SpPack (Perry, 2004). Quantitative color scale cluster maps based on univariate Getis and Franklin's local point pattern analysis method were generated using a custom MATLAB script as described previously (Owen et al., 2010) with a sampling radius of 50 nm. Two dimensional pseudo-color density maps were created by interpolating a surface plot with L(50) as the z-axis on a grid of resolution 5 nm. Binary maps, generated from density maps were used to measure cluster sizes and the number of clusters per μm^2 in ImageJ by using the particle analysis function. Varying label density analysis was performed as described previously (Baumgart et al., 2016).

Coordinate-based co-localization (CBC) analysis

CBC mediated analysis between two receptors was performed using an ImageJ plug-in (Ovesny et al., 2014) based on an algorithm described previously (Malkusch et al., 2012). To assess the correlation function for each localization, the x-y coordinate list from 488 nm and 647 nm dSTORM channels were used. For each localization from the 647 nm channel the correlation function to each localization from the 488 nm channel was calculated. This parameter can vary between -1 (perfectly segregated) through 0 (uncorrelated distributions) up to +1 (perfectly co-localized). The correlation coefficients were plotted as a histogram of occurrences with a 0.1 binning. The nearest neighbor distance (NND) between each localization from the 647 nm channel and its closest localization from the 488 nm channel was measured and plotted as the median NND between localizations per cell.

To assess protein cluster co-localization, centroid NND were calculated using an ImageJ plug-in as described above. Dual-color dSTORM images were converted into binary maps and the *x* and *y* coordinates of cluster centroids were identified in each image using the

particle analysis function in ImageJ. The NND from the centroid of a cluster in the 488 nm channel to the closest centroid of a cluster in the 647 nm channel was measured and plotted as a histogram of occurrences with a 10 nm binning. Experimental data were compared against randomized equivalents where the red (647 nm) channel images were randomly assigned new centroid coordinates within a region of interest delineating the cell boundary. The mode of the histograms was determined by fitting the distribution to a Gaussian function.

Statistical analysis

Samples were tested for normality with a Kolmogorov-Smirnov (K-S) test. The statistical significance of differences between two data sets was assessed by a two-tailed t-test assuming unequal variance; multiple comparisons were made with one-way ANOVA with Tukey's post-hoc test. All statistical analysis was performed using Origin software (OriginLab).

Online supplemental material

Fig. S1 shows the phenotyping of macrophages and the analysis of SIRPα, FcγRI and FcγRII surface expression by flow cytometry. Fig. S2 shows the nanometer-scale organization of SIRPα and FcγRI at 30 min of incubation. Fig. S3 shows the reorganization of FcγRI into concentric rings at the phagocytic synapse by confocal microscopy and isotype-matched control staining for all antibodies used in this study. Fig. S4 shows that the engagement of Fcγ receptors is required for their reorganization into concentric rings. Fig. S5 shows that SIRPα inhibition of FcγRI segregation and reorganization into concentric rings persists at 30 min of activation. Video 1 shows live TIRF imaging of the distribution of FcγRI at the surface of macrophages during cell spreading under non-activating conditions. Video 2 shows live TIRF imaging of the formation of FcγRI concentric rings at the surface of macrophages during cell spreading under activating conditions. Video 3 shows a

representative confocal Z-stack and 3D projection of the distribution of FcγRI at the surface of macrophages under activating conditions. Video 4 shows a representative confocal Z-stack and 3D projection of the distribution of FcγRI at the surface of macrophages under non-activating conditions.

Acknowledgements

We thank Kevin Stacey for the isolation of monocytes, other members of our laboratory for useful discussions, Rose Maciewicz for comments on the manuscript, and Gareth Howell for help with flow cytometry. This work was supported by the Medical Research Council (Award G1001044), a Wellcome Trust Investigator Award (110091) and the Manchester Collaborative Centre for Inflammation Research (funded by a pre-competitive open-innovation award from GSK, AstraZeneca and The University of Manchester, UK). The authors declare no competing financial interests.

Authorship Contributions

F.B.L. and S.B. performed all experiments and analyzed the data; S.V., J.H.F. and M.L.D. helped design and perform experiments involving supported lipid bilayers; F.B.L., S.B., E.M.H. and D.M.D. conceived the project; F.B.L., S.B. and D.M.D. designed experiments and wrote the manuscript.

References

1. Balint, S., I. Verdeny Vilanova, A. Sandoval Alvarez, and M. Lakadamyali. 2013. Correlative live-cell and superresolution microscopy reveals cargo transport dynamics at microtubule intersections. *PNAS*. 110:3375-3380.

2. Bates, M., B. Huang, G.T. Dempsey, and X. Zhuang. 2007. Multicolor Super-Resolution Imaging with Photo-Switchable Fluorescent Probes. *Science*. 317:1749-1753.

3. Bates, M., G.T. Dempsey, K.H. Chen, and X. Zhuang. 2012. Multicolor super-resolution fluorescence imaging via multi-parameter fluorophore detection. *ChemPhysChem*. 13:99-107.

4. Baumgart, F., A.M. Arnold, K. Leskovar, K. Staszek, M. Fölser, J. Weghuber, H. Stockinger, and G.J. Schütz. 2016. Varying label density allows artifact-free analysis of membrane-protein nanoclusters. *Nat. Methods*. 13:661-664.

5. Bruhns, P., B. Iannascoli, P. England, D.A. Mancardi, N. Fernandez, S. Jorieux, and M. Daëron. 2009. Specificity and affinity of human Fcγ receptors and their polymorphic variants for human IgG subclasses. *Blood*. 113:3716-3725.

6. Bunnell, S.C., D.I. Hong, J.R. Kardon, T. Yamazaki, C.J. McGlade, V.A. Barr, and L.E. Samelson. 2002. T cell receptor ligation induces the formation of dynamically regulated signaling assemblies. *J. Cell Biol*. 158:1263-1275

7. Cannon, G.J., and J.A. Swanson. 1992. The macrophage capacity for phagocytosis. *J. Cell Sci*. 101:907-913.

8. Chang, V.T., R.A. Fernandes, K.A. Ganzinger, S.F. Lee, C. Siebold, J. McColl, P. Jönsson, M. Palayret, K. Harlos, C.H. Coles, E.Y. Jones, Y. Lui, E. Huang, R.J.C. Gilbert, D. Klenerman, A.R. Aricescu, and S.J. Davis. 2016. Initiation of T cell signaling by CD45 segregation at "close contacts". *Nat. Immunol*. 17:574-582.

9. Davies, J.Q., and S. Gordon. 2005. Isolation and culture of human macrophages. *Methods Mol. Biol*. 290:105-16.

10. Davis, D.M., and M.L. Dustin. 2004. What is the importance of the immunological synapse? *Trends Immunol*. 25:323-327.

11. Dustin, M.L., T. Starr, R. Varma, and V.K. Thomas. 2007. Supported planar bilayers for study of the immunological synapse. *Curr. Protoc. Immunol*. Ch. 18, Unit 18.13.

12. Flannagan, R.S., V. Jaumouillié, and S. Grinstein. 2012. The cell biology of phagocytosis. *Annu. Rev. Pathol*. 7:61-98.

13. Freeman, S.A., J. Goyette, W. Furuya, E.C. Woods, C.R. Bertozzi, W. Bergmeier, B. Hinz, P.A. van der Merwe, R. Das, and S. Grinstein. 2016. Integrins form an expanding diffusional barrier that coordinates phagocytosis. *Cell*. 164:128-140.

14. Fujioka, Y., T. Matozaki, T. Noguchi, A. Iwamatsu, T. Yamao, N. Takahashi, M. Tsuda, T. Takada, and M. Kasuga. 1996. A novel membrane glycoprotein, SHPS-1, that binds the SH2-domain-containing protein tyrosine phosphatase SHP-2 in response to mitogens and cell adhesion. *Mol. Cell. Biol*. 16:6887-6899.

15. Getis, A., and J. Franklin. 1987. Second-order neighborhood analysis of mapped point patterns. *Ecology*. 68:473-477.

16. Ghazizadeh, S., J.B. Bolen, and H.B. Fleit. 1994. Physical and functional association of Src-related protein tyrosine kinases with Fc gamma RII in monocytic THP-1 cells. *J. Biol. Chem*. 269:8878-8884.

17. Griffin Jr, F.M., J.A. Griffin, J.E. Leider, and S.C. Silverstein. 1975. Studies on the mechanism of phagocytosis. I. Requirements for circumferential attachment of particle-bound ligands to specific receptors on the macrophage plasma membrane. *J. Exp. Med*. 142:1263-1282.

18. Harwood, N.E., and F.D. Batista. 2008. New insights into early molecular events underlying B cell activation. *Immunity*. 28:609-619.

19. Heilemann, M., S. van der Linde, M. Schuttpelz, R. Kasper, B. Seefeldt, A. Mukherjee, P. Tinnefeld, and M. Sauer. 2008. Subdiffraction-resolution fluorescence imaging with conventional fluorescent probes. *Angew. Chem. Int. Ed*. 47:6172-6176.

20. Heiple, J.M., S.D. Wright, N.S. Allen, and S.C. Silverstein. 1990. Macrophages form circular zones of very close apposition to IgG-coated surfaces. Cell Motil. *Cytoskeleton*. 15:260-270.

21. Huang, B., W. Wang, M. Bates, and X. Zhuang. 2008. Three-Dimensional Super-Resolution Imaging by Stochastic Optical Reconstruction Microscopy. *Science*. 319:810-813

22. Jaumouillé, V., and S. Grinstein. 2011. Receptor mobility, the cytoskeleton, and particle binding during phagocytosis. *Curr. Opin. Cell Biol*. 23:22-29

23. Jaumouillé, V., Y. Farkash, K. Jaqaman, R. Das, C.A. Lowell, and S. Grinstein. 2014. Actin Cytoskeleton Reorganization by Syk Regulates Fcγ Receptor Responsiveness by Increasing Its Lateral Mobility and Clustering. *Dev. Cell*. 29:534-546.

24. Jiang, P., C.F. Lagenaur, and V. Narayanan. 1999. Integrin-associated protein is a ligand for the P84 neural adhesion molecule. *J. Biol. Chem*. 274:559-562.

25. Klasener, K., P.C. Maity, E. Hobeika, J. Yang, and M. Reth. 2014. B cell activation involves nanoscale receptor reorganizations and inside-out signaling by Syk. *Elife*. 3:e02069.

26. Lagrue, K., A. Carisey, A. Oszmiana, P.R. Kennedy, D.J. Williamson, A. Cartwright, C. Barthen, and D.M. Davis. 2013. The central role of the cytoskeleton in mechanisms and functions of the NK cell immune synapse. *Immunol. Rev*. 256:203-211.

27. Lillemeier, B.F., M.A. Mörtelmaier, M.B. Forstner, J.B. Huppa, J.T. Groves, and M.M. Davis. 2010. TCR and Lat are expressed on separate protein islands on T cell membranes and concatenate during activation. *Nat. Immunol*. 11:90-96.

28. Malkusch, S., U. Endesfelder, J. Mondry, M. Gelléri, P.J. Verveer, and M. Heilemann. 2012. Coordinate-based colocalization analysis of single-molecule localization microscopy data. *Histochem. Cell Biol*. 137:1-10.

29. Mattila, P.K., C. Feest, D. Depoil, B. Treanor, B. Montaner, K.L. Otipoby, R. Carter, L.B. Justement, A. Bruckbauer, and F.D. Batista. 2013. The Actin and Tetraspanin Networks Organize Receptor Nanoclusters to Regulate B Cell Receptor-Mediated Signaling. *Immunity*. 38:461-474.

30. Okazawa, H., S. Motegi, N. Ohyama, H. Ohnishi, T. Tomizawa, Y. Kaneko, P.A. Oldenborg, O. Ishikawa, and T. Matozaki. 2005. Negative regulation of phagocytosis in macrophages by the CD47-SHPS-1 system. *J. Immunol*. 174:2004-2011.

31. Oldenborg, P.A., A. Zheleznyak, Y.F. Fang, C.F. Lagenaur, H.D. Gresham, and F.P. Lindberg. 2000. Role of CD47 as a marker of self on red blood cells. *Science*. 288:2051-2054.

32. Oldenborg, P.A., H.D. Gresham, and F.P. Lindberg. 2001. CD47-signal regulatory protein alpha (SIRPalpha) regulates Fcgamma and complement receptor-mediated phagocytosis. *J. Exp. Med*. 193:855-862.

33. Orange, J.S. 2008. Formation and function of the lytic NK-cell immunological synapse. *Nat. Rev. Immunol*. 8:713-725.

34. Ovesny, M., P. Krizek, J. Borkovec, Z. Svindrych, and G.M. Hagen. 2014. ThunderSTORM: a comprehensive ImageJ plug-in for PALM and STORM data analysis and super-resolution imaging. *Bioinformatics*. 30:2389-2390.

35. Owen, D.M., C. Rentero, J. Rossy, A. Magenau, D. Williamson, M. Rodriguez, and K. Gaus. 2010. PALM imaging and cluster analysis of protein heterogeneity at the cell surface. *J. Biophotonics*. 3:446-454.

36. Pageon, S.V., S.P. Cordoba, D.M. Owen, S.M. Rothery, A. Oszmiana, and D.M. Davis. 2013. Superresolution microscopy reveals nanometer-scale reorganization of inhibitory natural killer cell receptors upon activation of NKG2D. *Sci. Signal*. 6:ra62.

37. Parajo-Garcia, M.F., A. Cambi, J.A. Torreno-Pina, N. Thompson, and K. Jacobson. 2014. Nanoclustering as a dominant feature of plasma membrane organization. *J. Cell Sci*. 127:4995-5005.

38. Perry, G.L.W. 2004. SpPack: spatial point pattern analysis in Excel using Visual Basic for Applications (VBP). *Environ. Model. Softw*. 19:559-569.

39. Ripley, B.D. 1977. Modeling Spatial Patterns. *J. R. Stat. Soc. Ser. B Stat. Methodol*. 39:172-212.

40. Tsai, R.K., and D.E. Discher. 2008. Inhibition of "self" engulfment through deactivation of myosin-II at the phagocytic synapse between human cells. *J. Cell Biol*. 180:989-1003.

41. Veillette, A., E. Thibaudeau, and S. Latour. 1998. High expression of inhibitory receptor SHPS-1 and its association with protein-tyrosine phosphatase SHP-1 in macrophages. *J. Biol. Chem*. 273:22719-22728.

42. Wang, A.V., P.R. Scholl, and R.S. Geha. 1994. Physical and functional association of the high affinity immunoglobulin G receptor (FcγRI) with the kinases Hck and Lyn. *J. Exp. Med*. 180:1165-1170.

43. Williamson, D.J., D.M. Owen, J. Rossy, A. Magenau, M. Wehrmann, J.J. Gooding, and K. Gaus. 2011. Pre-existing clusters of the adaptor Lat do not participate in signaling events. *Nat. Immunol*. 12:655-662.

44. Yamauchi, S., K. Kawauchi, and Y. Sawada. 2012. Myosin II-dependent exclusion of CD45 from the site of Fcg receptor activation during phagocytosis. *FEBS Lett*. 586:3229-3235.

Figure Legends

Figure 1. SIRPα and FcγRI are arranged in discrete nanoclusters at macrophage surfaces.

(A and B) TIRF and dSTORM images of SIRPα (A) and FcγRI (B) at the surface of human macrophages seeded onto PLL- (non-activated, top row) or hIgG-coated slides (bottom row) for 10 min, and stained with fluorescently labeled specific antibodies. Scale bars, 5 μm. Regions delineated by white squares are zoomed-in and shown with corresponding density maps (pseudocolor scale), thresholded binary maps and Ripley's K analysis of the molecules in the selected regions. Scale bars, 1 μm. L(r)-r represents the degree of clustering relative to simulated random distributions, indicated by the 99% confidence intervals (CIs); r is the radial scale. (C) Nanocluster areas, (D) density, and (E) percentage of localizations in nanoclusters for SIRPα and FcγRI under non-activating (black) or hIgG-activating (grey) conditions were calculated by subjecting dSTORM data to spatial point-pattern analysis and thresholding. Each symbol represents the median of several 5 μm x 5 μm regions from the same cell. Horizontal lines and error bars represent mean ± SD. Data are from a minimum of 30 cells from 3 independent donors. ns, not significant. ****($p<0.0001$), two-tailed t-test assuming unequal variance. (F and G) Label-density variation analysis for SIRPα (F) and FcγRI (G) yields characteristic normalized ρ/η curves for clustered proteins. Cells were stained with anti-SIRPα-AF647 (F) or anti-FcγRI-AF488 (G) at different labeling concentrations and imaged by dSTORM. Each data point represents a single cell, color-coded by antibody concentration used for labeling. Red lines indicate reference curves for a random distribution of molecules.

Figure 2. SIRPα and FcγRI nanoclusters are constitutively associated in non-activated human macrophages but segregate upon activation with hIgG.

(A) TIRF and dSTORM images showing FcγRI (green) and SIRPα (red) at the surface of human macrophages incubated for 10 min on slides coated with PLL (non-activated, top

row) or hIgG (middle row), and stained with anti-FcγRI-AF488 and anti-SIRPα-AF647 mAbs. Scale bars, 5 μm. Regions outlined by the white squares (middle column) are shown enlarged (right columns) with relative fluorescence intensity profiles along the white lines. Scale bars, 1 μm. As a positive control, macrophages seeded onto PLL-coated slides were stained with anti-FcγRI-AF488 mAb followed by anti-mouse IgG1-AF647 secondary antibody (bottom row). (B) CBC histograms of the single-molecule distributions of the colocalization parameter for SIRPα and FcγRI in cells seeded onto PLL- (grey) or hIgG-coated (red) slides for 10 min, or for positive control data (green). Data are from a minimum of 30 cells from 3 independent donors. Bars represent mean ± SD. (C) Nearest-neighbor (NN) analysis from data shown in (B). Each symbol represents the median NN of all paired single-molecule localizations from one cell. Horizontal lines and error bars represent mean ± SD. ****($p<0.0001$), two-tailed t-test assuming unequal variance. (D) Histogram distributions of the NND between the centroids of nanoclusters from one channel and the centroid of their nearest neighbor from the second channel (≥ 20,000 clusters from a minimum of 10 cells per condition) from cells seeded onto PLL- (light grey), hIgG-coated (light red) slides, or positive control data (green). Corresponding simulated data is also shown, in which the centroid positions of SIRPα nanoclusters in both non-activating (dark grey) or hIgG-activating conditions (dark red) were randomized within the cell area.

Figure 3. The low-affinity Fc receptor FcγRII is arranged in discrete nanoclusters at macrophage surfaces.

(A and B) TIRF and dSTORM images of FcγRII at the surface of human macrophages seeded onto PLL- (non-activated) or hIgG-coated slides for 10 min (A) or 30 min (B), and stained with a fluorescently labeled specific antibody. Scale bars, 5 μm. Regions delineated by the white squares are zoomed-in and shown with corresponding density maps, binary maps and Ripley's K analysis. Scale bars, 1 μm. (C) Nanocluster areas, (D) density, and (E) percentage of localizations in nanoclusters for FcγRII under non-activated (black) or hIgG-activated (grey) conditions at 10 or 30 min were calculated as in Figure 1. Horizontal lines

and error bars represent mean ± SD. Data are from a minimum of 30 cells from 3 independent donors. ns, not significant. *($p<0.05$), **($p<0.01$), ****($p<0.0001$), two-tailed t-test assuming unequal variance.

Figure 4. SIRPα and the low-affinity Fc receptor, FcγRII, are segregated at nanometer-scale.

(A) TIRF and dSTORM images showing FcγRII (green) and SIRPα (red) at the surface of human macrophages incubated for 10 or 30 min on slides coated with PLL (non-activated) or hIgG, and stained with anti-FcγRII-AF488 and anti-SIRPα-AF647 mAbs. Scale bars, 5 μm. In each condition, regions outlined by the white squares (middle column) are shown enlarged (right column) with relative fluorescence intensity profiles along the white lines. Scale bars, 1 μm. (B) CBC histograms of the single-molecule distributions of the colocalization parameter for SIRPα and FcγRII in cells seeded onto PLL- or hIgG-coated slides for 10 (light grey and dark grey, respectively) or 30 min (light red and dark red, respectively), or for positive control data (green). The positive control data in this figure is the same as in Figure 2. Data are from a minimum of 30 cells from 3 independent donors. Bars represent mean ± SD. (C) NND analysis from data shown in (B). Each symbol represents the median NND of all paired single-molecule localizations from one cell. Horizontal lines and error bars represent mean ± SD. ns, not significant. **($p<0.01$), ***($p<0.001$), one-way ANOVA with Tukey's post-hoc test. (D) Histogram distributions of the NND between the centroids of nanoclusters from one channel and the centroid of their nearest neighbor from the second channel (≥ 20,000 clusters from a minimum of 10 cells per condition).

Figure 5. Fcγ receptors reorganize into concentric rings upon activation.

(A) TIRF images of FcγRI (top row) and FcγRII (bottom row) at the surface of human macrophages incubated for 10 or 30 min on slides coated with PLL (non-activated) or hIgG, and stained with fluorescently labeled specific antibodies. Scale bars, 10 μm. (B) TIRF and dSTORM images of FcγRI (green) and FcγRII (red) at the surface of macrophages

incubated for 10 or 30 min on slides coated with PLL or hIgG, and stained with anti-FcγRI-AF488 and anti-FcγRII-AF647 mAbs. Scale bars, 5 μm. Regions outlined by the white squares (middle column) are shown enlarged (right column) with relative fluorescence intensity profiles along the white lines. Scale bars, 1 μm. (C) CBC histograms of the single-molecule distributions of the colocalization parameter for FcγRI and FcγRII in cells seeded onto PLL- or hIgG-coated slides for 10 (light grey and dark grey, respectively) or 30 min (light red and dark red, respectively), or for positive control data (green). The positive control data in this figure is the same as in Figure 2. Data are from a minimum of 30 cells from 3 independent donors. Bars represent mean ± SD. (D) NND analysis from data shown in (C). Each symbol represents the median NND of all paired single-molecule localizations from one cell. Horizontal lines and error bars represent mean ± SD. ns, not significant. **($p<0.01$), ****($p<0.0001$), one-way ANOVA with Tukey's post-hoc test. (E) Histogram distributions of the NND between the centroids of nanoclusters from one channel and the centroid of their nearest neighbor from the second channel (≥ 20,000 clusters from a minimum of 10 cells per condition).

Figure 6. Specific activation of FcγRI is required for its reorganization into concentric rings and segregation from SIRPα nanoclusters.

(A and B) TIRF (scale bars, 10 μm) and dSTORM (scale bars, 5 μm) images showing FcγRI (green) and SIRPα (red) at the surface of human macrophages incubated for 10 (A) or 30 min (B) on slides coated with hIgG1 or hIgG2, and stained with anti-FcγRI-AF488 and anti-SIRPα-AF647 mAbs. In each condition, regions outlined by the white squares (middle column) are shown enlarged (right column) with relative fluorescence intensity profiles along the white lines. Scale bars, 1 μm. (C) CBC histograms of the single-molecule distributions of the colocalization parameter for FcγRI and SIRPα in cells seeded onto hIgG1- or hIgG2-coated slides for 10 (light grey and dark grey, respectively) or 30 min (light red and dark red, respectively). Data are from a minimum of 30 cells from 3 independent donors. Bars represent mean ± SD. (D) NND analysis from data shown in (C). Each symbol represents

the median NND of all paired single-molecule localizations from one cell. Horizontal lines and error bars represent mean ± SD. ns, not significant. **(p<0.01), ****(p<0.0001), one-way ANOVA with Tukey's post-hoc test. (E) Histogram distributions of the NND between the centroids of nanoclusters from one channel and the centroid of their nearest neighbor from the second channel (≥ 20,000 clusters from a minimum of 10 cells per condition).

Figure 7. Rearrangement of macrophage surface receptors triggered by mobile hIgG.

(A) TIRF images of FcγRI at the surface of human macrophages incubated for 10 min on supported lipid bilayers loaded with streptavidin (non-activating) or with streptavidin-hIgG (activating), and stained with a fluorescently labeled specific antibody. Two example images are shown for each condition. Scale bars, 10 µm. (B) dSTORM images of FcγRI (green) and SIRPα (red) at the surface of macrophages seeded as in (A), and stained with anti-FcγRI-AF488 and anti-SIRPα-AF647 mAbs. Scale bars, 5 µm. Regions outlined by the white squares are shown enlarged with relative fluorescence intensity profiles along the white lines. Scale bars, 1 µm. (C) Nanocluster areas, (D) density, and (E) percentage of localizations in nanoclusters for SIRPα and FcγRI under non-activating (black) or hIgG-activating (grey) conditions. Each symbol represents the median of several 5 µm x 5 µm regions from the same cell. Horizontal lines and error bars represent mean ± SD. Data are from a minimum of 30 cells from two independent experiments. ns, not significant. *(p<0.05), ****(p<0.0001), two-tailed t-test assuming unequal variance. (F) CBC histograms of the single-molecule distributions of the colocalization parameter for SIRPα and FcγRI in cells seeded as in (A). Data are from a minimum of 30 cells from two independent experiments. Bars represent mean ± SD. (G) NND analysis from data shown in (F). Each symbol represents median NND of all paired single-molecule localizations from one cell. Horizontal lines and error bars represent mean ± SD. ****(p<0.0001), two-tailed t-test assuming unequal variance. (H) Histogram distributions of the NND between the centroids of nanoclusters from one channel and the centroid of their nearest neighbor from the second

channel (≥ 10,000 clusters from a minimum of 10 cells per condition) from cells seeded onto control non-activating (light grey) or hIgG-loaded activating (light red) SLB.

Figure 8. Ligation of SIRPα impairs the reorganization of surface FcγRI.

(A) Human macrophages were incubated for 24 hours in wells coated with PLL, 20 µg/ml of hCD47 or with increasing concentrations of hCD47 in the presence of 10 µg/ml of hIgG, as indicated. M-CSF release was assessed by ELISA. Bars represent mean ± SD from 3 donors. Each color represents one individual donor. (B) TIRF images of FcγRI at the surface of human macrophages incubated for 10 min on slides coated with hCD47 or hCD47 + hIgG, and stained with fluorescently labeled specific antibody. Scale bars, 10 µm. (C) TIRF and dSTORM images showing FcγRI (green) and SIRPα (red) at the surface of human macrophages incubated for 10 min on slides coated with hCD47 (top row) or hCD47 + hIgG (bottom row), and stained with anti-FcγRI-AF488 and anti-SIRPα-AF647 mAbs. Scale bars, 5 µm. In each condition, regions outlined by the white squares (middle column) are shown enlarged (right column) with relative fluorescence intensity profiles along the white lines. Scale bars, 1 µm. (D and G) CBC histograms of the single-molecule distributions of the colocalization parameter for FcγRI and SIRPα (D) and for FcγRI and pSHP-1^{Y536} (G) in cells seeded onto slides coated with PLL (light grey), hCD47 (light red), hCD47 + hIgG (dark red) or hIgG (dark grey) for 10 (D) or 5 min (G). Data are from a minimum of 30 cells from 3 independent donors. Bars represent mean ± SD. (E and H) NND analysis from data shown in (D and G). Each symbol represents the median NND of all paired single-molecule localizations from one cell. Horizontal lines and error bars represent mean ± SD. ns, not significant. ****($p<0.0001$), one-way ANOVA with Tukey's post-hoc test. (F and I) Histogram distributions of the NND between the centroids of nanoclusters from one channel and the centroid of their nearest neighbor from the second channel (≥ 20,000 clusters from a minimum of 10 cells per condition).

Figure 9. Segregation and reorganization of FcγRI is dependent on the actin cytoskeleton and formins, not myosin II.

(A) TIRF image of FcγRI (white, scale bars, 20 μm) and dSTORM images (scale bars, 5 μm) of FcγRI (green) and SIRPα (red) at the surface of human macrophages pre-treated with 1 μM Lat A, 0.5 μM Jasp, 10 μM Bleb or 10 μM SMIFH2. Cells were then seeded onto slides coated with PLL (non-activated) or hIgG for 10 min, and stained with anti-FcγRI-AF488 and anti-SIRPα-AF647 mAbs. In each condition, regions outlined by the white squares (middle column) are shown enlarged (right column). Scale bars, 1 μm. (B) CBC histograms of the single-molecule distributions of the colocalization parameter for FcγRI and SIRPα in cells pre-treated with drugs as indicated and seeded onto slides coated with PLL (grey) or hIgG (Lat A – dark grey, Jasp – red, SMIFH2 - green, or Bleb - blue) for 10 min. Data are from a minimum of 30 cells per condition from 3 independent donors. Bars represent mean ± SD. (C) NND analysis from data shown in (B). Each symbol represents the median NND of all paired single-molecule localizations from one cell. Horizontal lines and error bars represent mean ± SD. ns, not significant. **($p<0.01$), ****($p<0.0001$), two-tailed t-test assuming unequal variance. (D) Histogram distributions of the NND between the centroids of nanoclusters from one channel and the centroid of their nearest neighbor from the second channel (≥ 20,000 clusters from a minimum of 10 cells per condition). (E) Nanocluster areas, (F) density, and (G) percentage of localizations in nanoclusters for SIRPα and FcγRI under non-activating (black) or hIgG-activating (grey) conditions after pre-treatment of cells with blebbistatin or DMSO control. Each symbol represents the median of several 5 μm x 5 μm regions from the same cell. Horizontal lines and error bars represent mean ± SD. Data are from a minimum of 30 cells from 3 independent donors. ns, not significant. *($p<0.05$), **($p<0.01$), ***($p<0.001$), ****($p<0.0001$), two-tailed t-test assuming unequal variance.

Figure 10. Src-family kinase signaling, but not Syk- or PI3K-signaling, is indispensable for reorganization of macrophage surfaces.

(A) Immunoblots of phosphorylated AKT in non-activated (PLL) or hIgG-activated human macrophages pre-treated with vehicle (DMSO), as a control, 10 μM PP2 (left panel), 100 μM piceatannol (PCT, middle panel) or 1 μM wortmannin (Wort, right panel). Blots represent two independent experiments. (B) TIRF image of FcγRI (white, scale bars, 20 μm) and dSTORM images (scale bars, 5 μm) of FcγRI (green) and SIRPα (red) at the surface of human macrophages incubated with vehicle (DMSO), PP2, PCT or Wort, pre-treated as in (A). Cells were then seeded onto slides coated with PLL (non-activated) or hIgG for 10 min, and stained with anti-FcγRI-AF488 and anti-SIRPα-AF647 mAbs. In each condition, regions outlined by the white squares (middle column) are shown enlarged (right column). Scale bars, 1 μm. (C) CBC histograms for FcγRI and SIRPα in cells pre-treated as in (A) and seeded onto slides coated with PLL (grey) or hIgG (DMSO – dark grey, PP2 - red, PCT - green and Wort - blue) for 10 min, as indicated. Data are from a minimum of 30 cells from 3 independent donors. Bars show mean ± SD. (D) NND analysis from data shown in (C). Each symbol represents the median NND of all paired single-molecule localizations from one cell. Horizontal lines and error bars represent mean ± SD. ns, not significant. ****($p<0.0001$), one-way ANOVA with Tukey's post-hoc test. (E) Histogram distributions of the NND between the centroids of nanoclusters from one channel and the centroid of their nearest neighbor from the second channel (≥ 20,000 clusters from a minimum of 10 cells per condition).

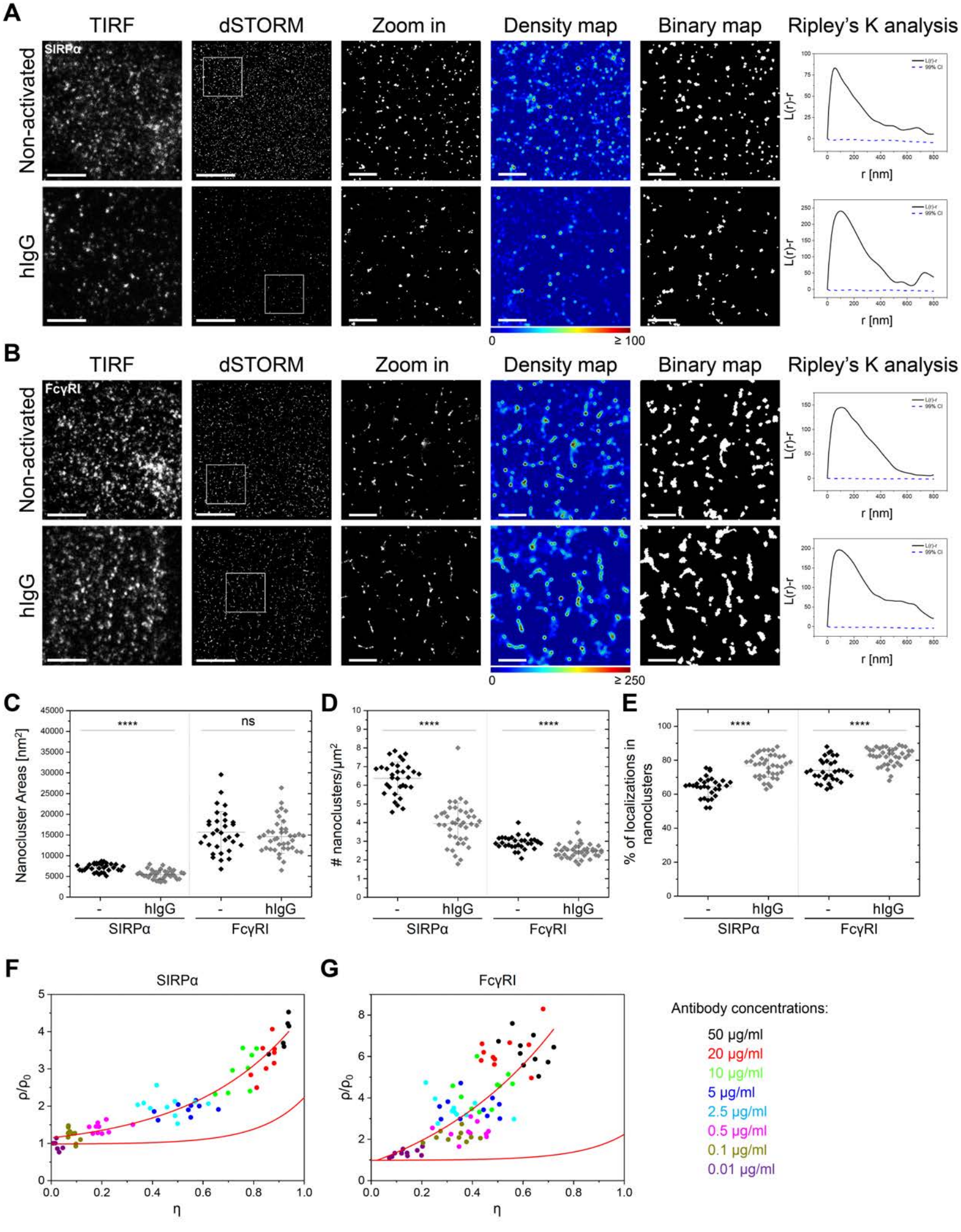
A
TIRF
dSTORM
Zoom in
Density map
Binary map
Ripley's K analysis
Non-activated
hIgG
SIRPα
0
≥ 100
r [nm]
L(r)-r
B
FcγRI
≥ 250
C
Nanocluster Areas [nm²]
****
ns
D
nanoclusters/µm²
E
% of localizations in nanoclusters
-
hIgG
SIRPα
FcγRI
F
SIRPα
ρ/ρ0
η
G
FcγRI
Antibody concentrations:
50 µg/ml
20 µg/ml
10 µg/ml
5 µg/ml
2.5 µg/ml
0.5 µg/ml
0.1 µg/ml
0.01 µg/ml

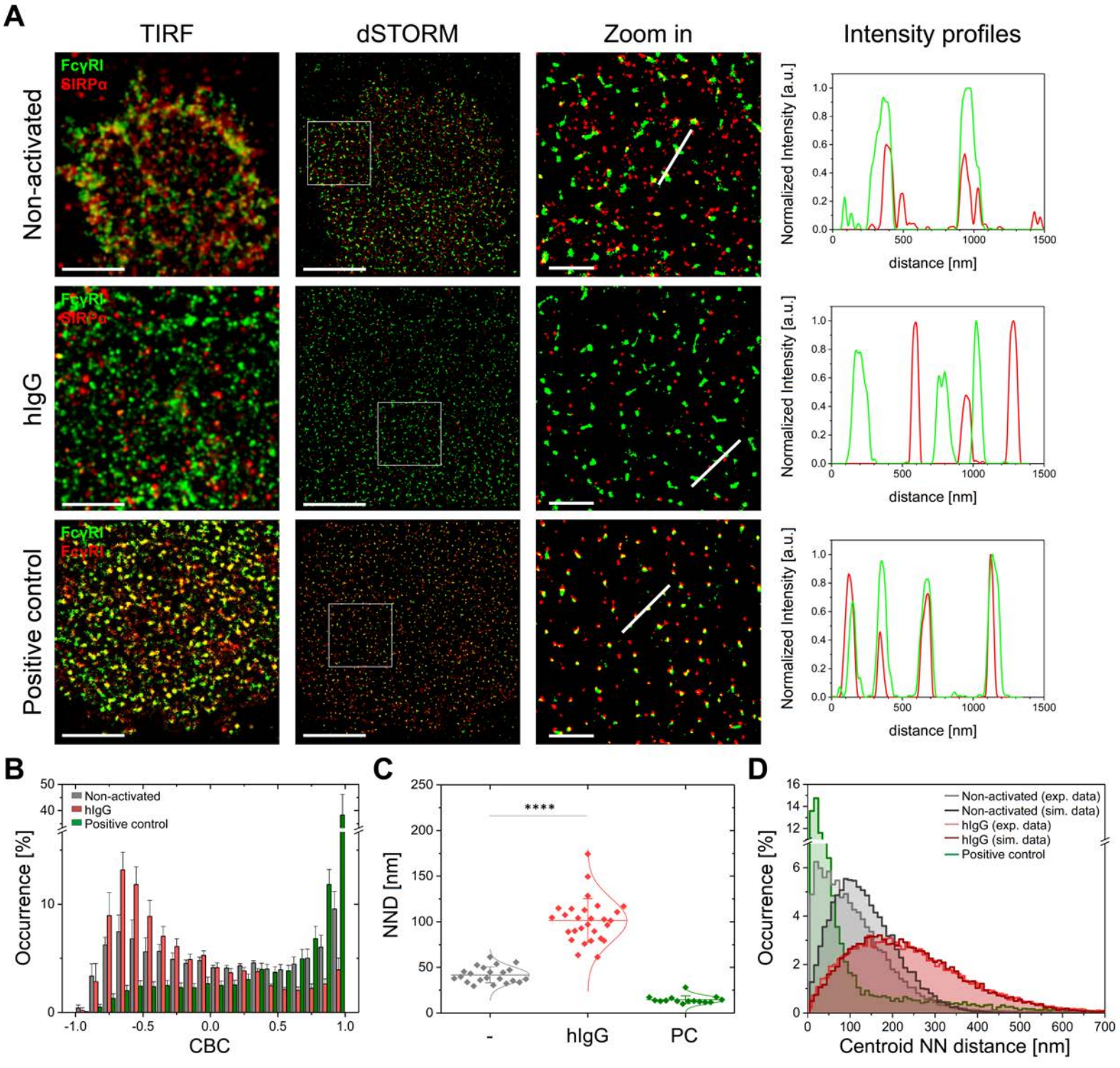
A
TIRF
dSTORM
Zoom in
Intensity profiles
Non-activated
hIgG
Positive control
FcγRI
SIRPα
FcγRI
FcγRI
Normalized Intensity [a.u.]
distance [nm]
B
Non-activated
hIgG
Positive control
Occurrence [%]
CBC
C
****
NND [nm]
-
hIgG
PC
D
Non-activated (exp. data)
Non-activated (sim. data)
hIgG (exp. data)
hIgG (sim. data)
Positive control
Occurrence [%]
Centroid NN distance [nm]

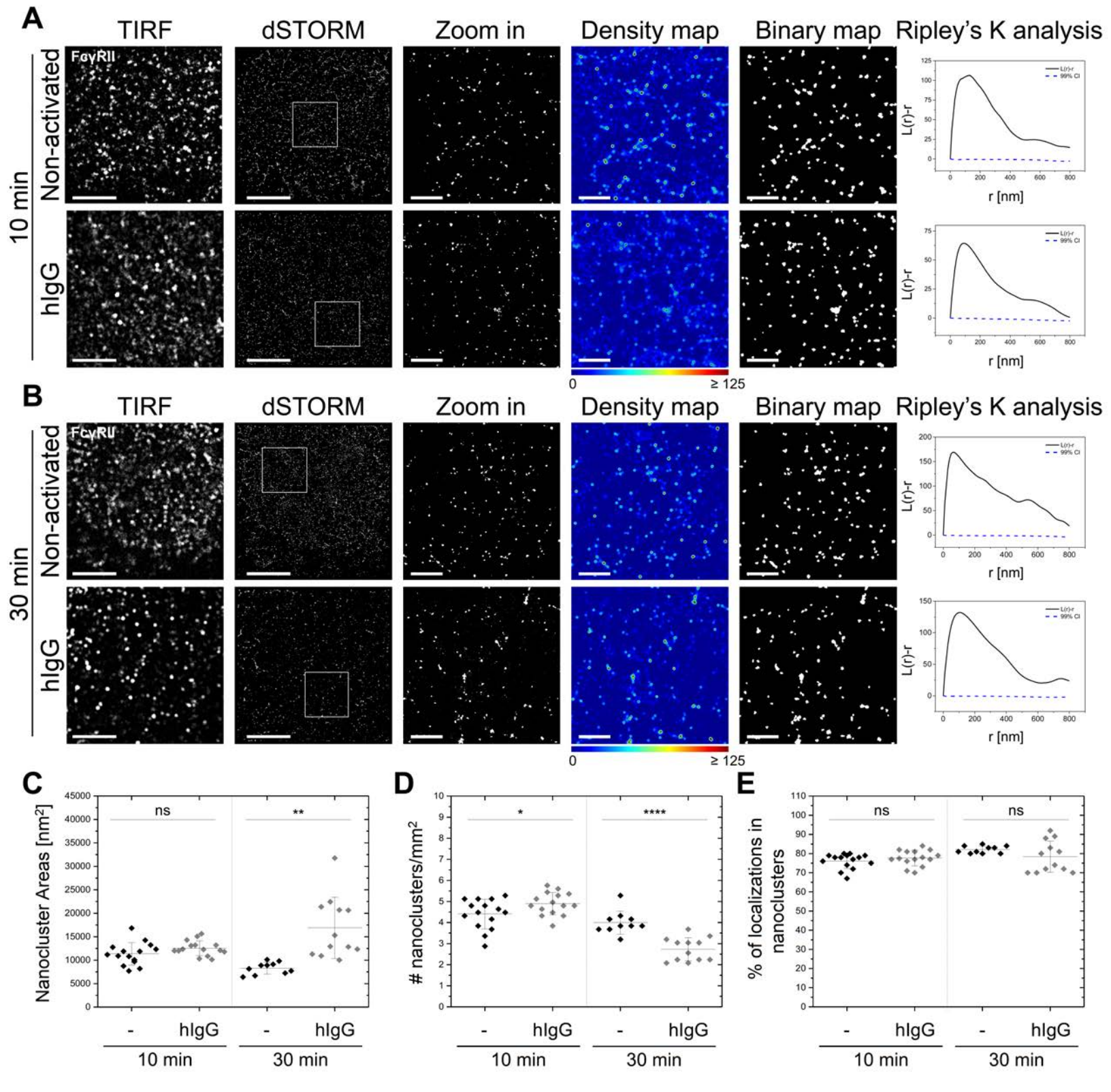
A
TIRF
dSTORM
Zoom in
Density map
Binary map
Ripley's K analysis
10 min
Non-activated
hIgG
FcγRII
0
≥ 125
L(r)-r
r [nm]
B
30 min
C
Nanocluster Areas [nm²]
ns
**
D
nanoclusters/mm²
*
****
E
% of localizations in nanoclusters
ns
ns
-
hIgG
10 min
30 min

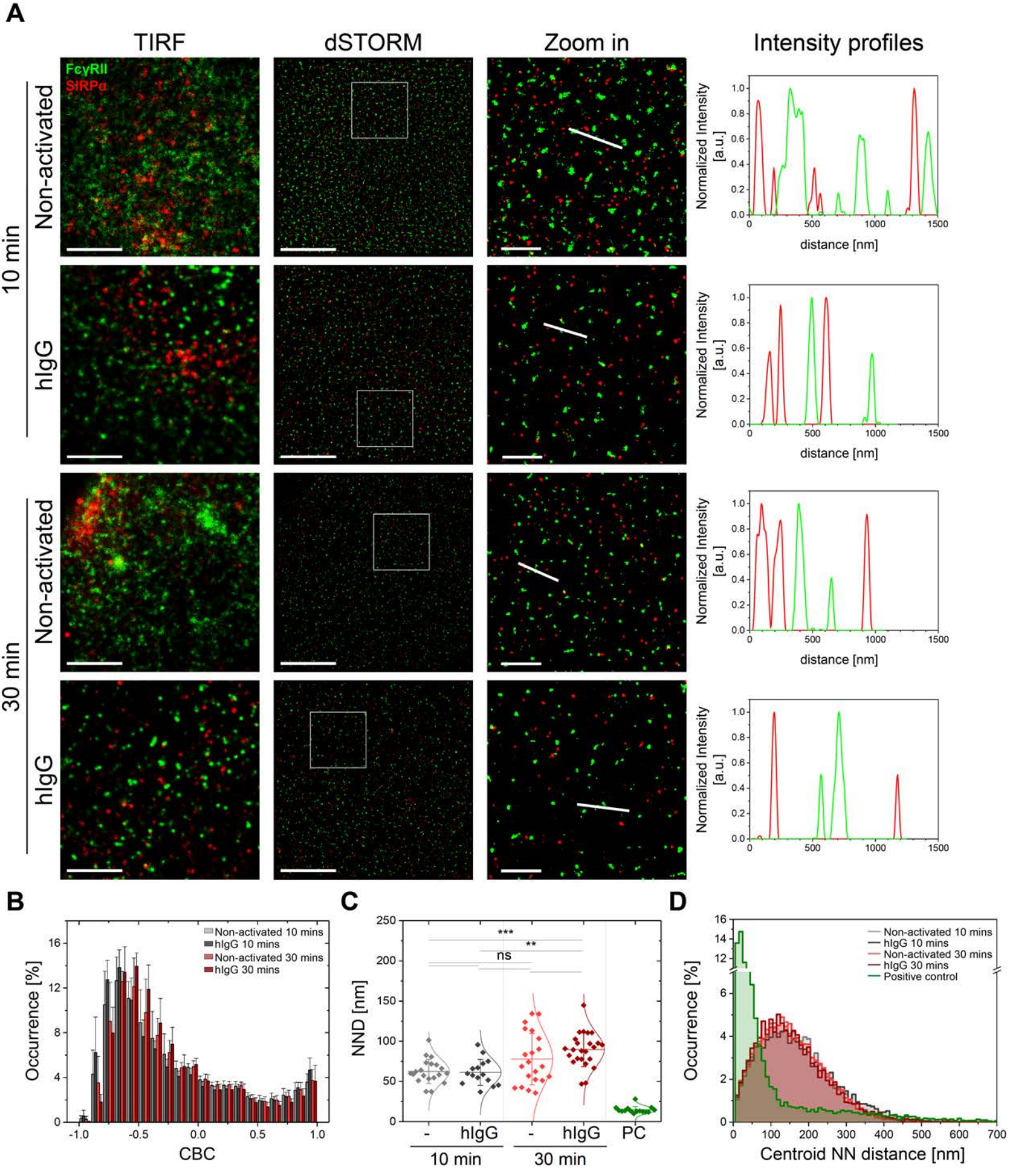
A
TIRF
dSTORM
Zoom in
Intensity profiles
FcγRII
SIRPα
10 min
30 min
Non-activated
hIgG
Normalized Intensity [a.u.]
distance [nm]
B
Non-activated 10 mins
hIgG 10 mins
Non-activated 30 mins
hIgG 30 mins
Occurrence [%]
CBC
C
NND [nm]
***
**
ns
-
hIgG
PC
10 min
30 min
D
Positive control
Occurrence [%]
Centroid NN distance [nm]

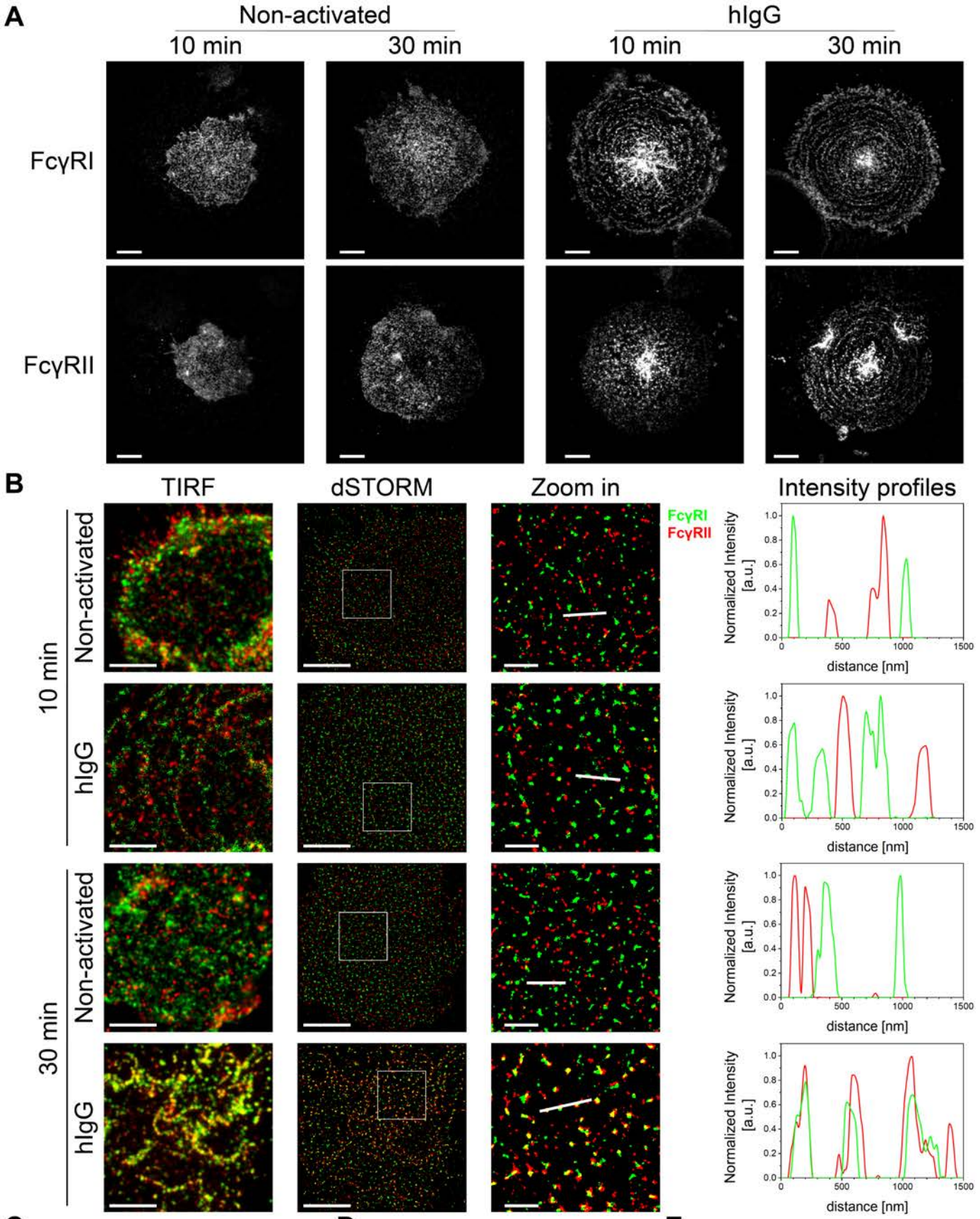
A
Non-activated
hIgG
10 min
30 min
10 min
30 min
FcγRI
FcγRII
B
TIRF
dSTORM
Zoom in
Intensity profiles
FcγRI
FcγRII
10 min
Non-activated
hIgG
30 min
Non-activated
hIgG
Normalized Intensity [a.u.]
distance [nm]
C
Non-activated 10 mins
hIgG 10 mins
Non-activated 30 mins
hIgG 30 mins
Positive control
Occurrence [%]
CBC
D
NND [nm]
ns
**
****
-
hIgG
-
hIgG
PC
10 min
30 min
E
Non-activated 10 mins
hIgG 10 mins
Non-activated 30 mins
hIgG 30 mins
Positive control
Occurrence [%]
Centroid NN distance [nm]

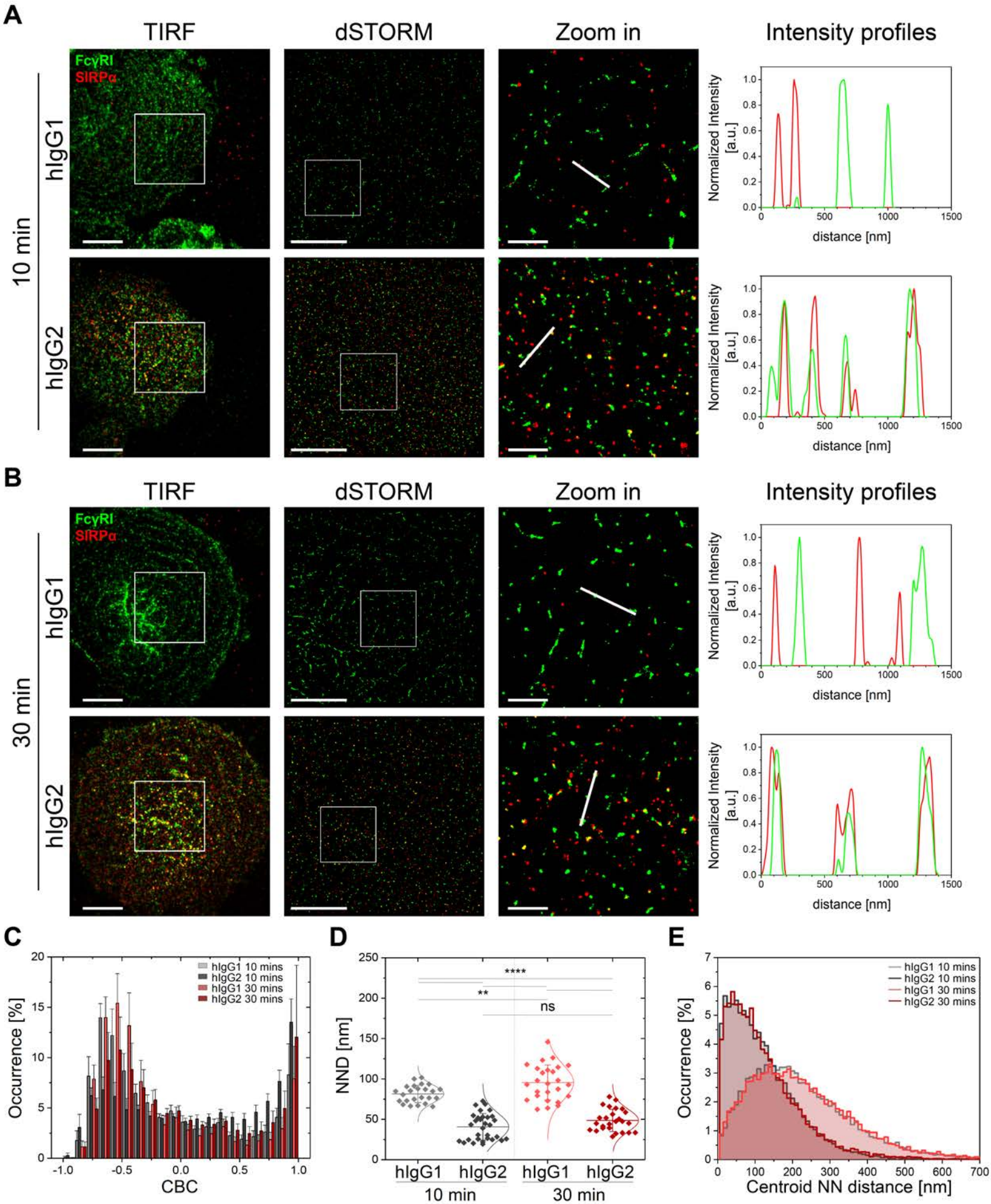
A
TIRF
dSTORM
Zoom in
Intensity profiles
FcγRI
SIRPα
hIgG1
hIgG2
10 min
Normalized Intensity [a.u.]
distance [nm]
B
30 min
C
Occurrence [%]
CBC
hIgG1 10 mins
hIgG2 10 mins
hIgG1 30 mins
hIgG2 30 mins
D
NND [nm]
****
**
ns
10 min
30 min
E
Centroid NN distance [nm]

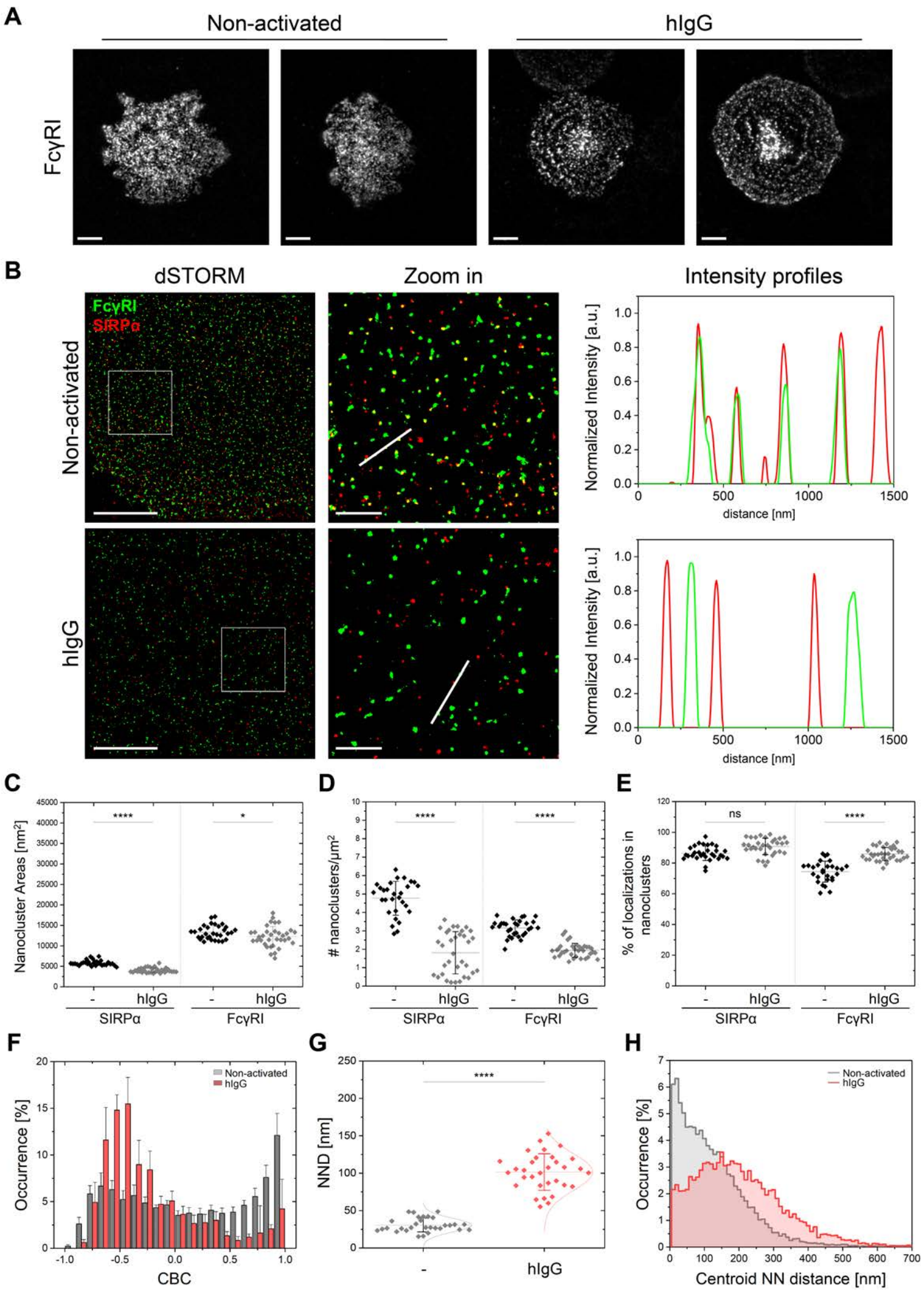
A
Non-activated
hIgG
FcγRI
B
dSTORM
Zoom in
Intensity profiles
FcγRI
SIRPα
Non-activated
hIgG
Normalized Intensity [a.u.]
distance [nm]
C
Nanocluster Areas [nm²]
****
*
-
hIgG
SIRPα
FcγRI
D
nanoclusters/µm²
****
E
% of localizations in nanoclusters
ns
F
Occurrence [%]
Non-activated
hIgG
CBC
G
NND [nm]
H
Centroid NN distance [nm]

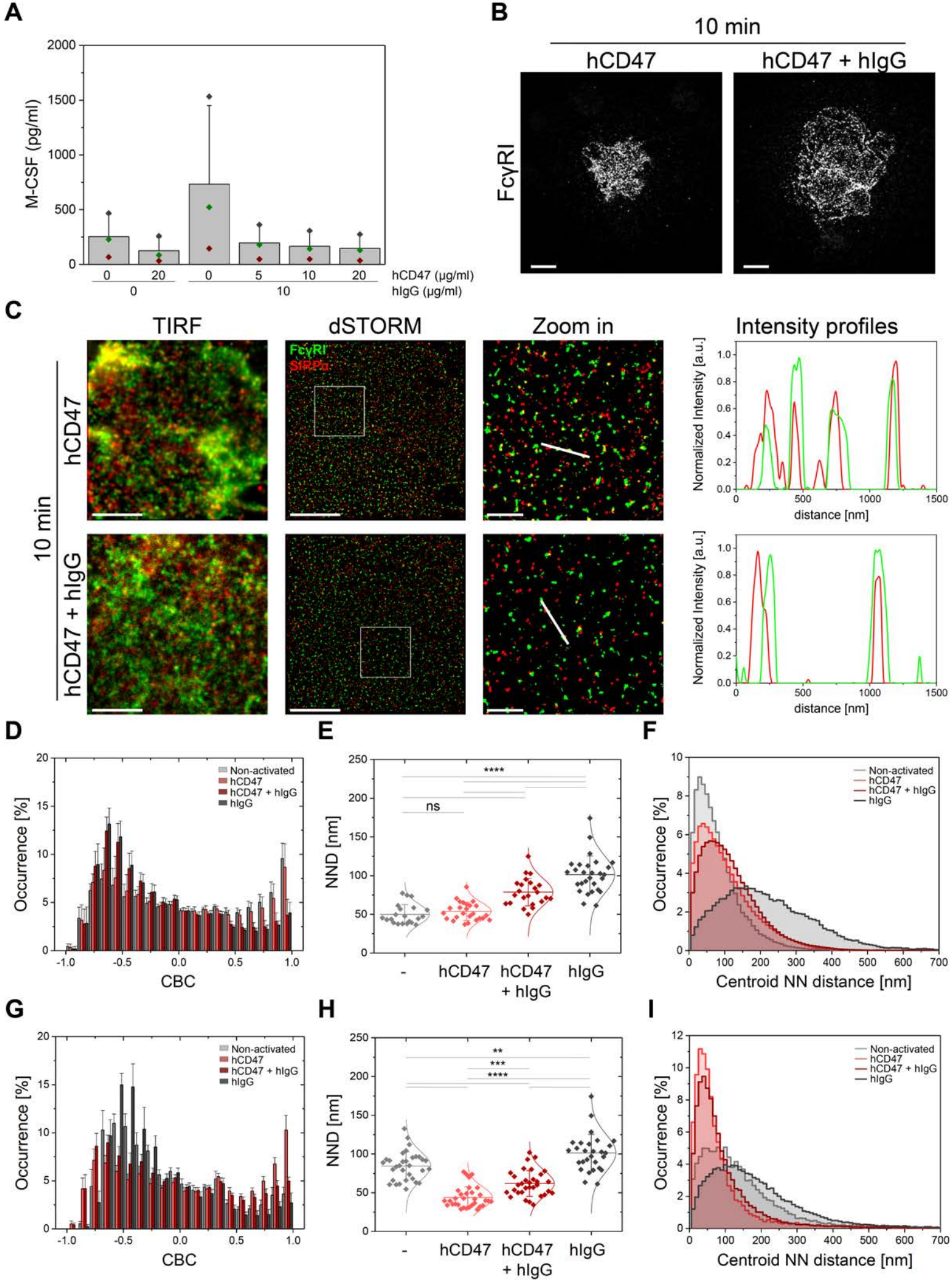
A
M-CSF (pg/ml)
2000
1500
1000
500
0
0
20
0
5
10
20
hCD47 (µg/ml)
0
10
hIgG (µg/ml)
B
10 min
hCD47
hCD47 + hIgG
FcγRI
C
TIRF
dSTORM
Zoom in
Intensity profiles
10 min
hCD47
hCD47 + hIgG
FcγRI
SIRPα
Normalized Intensity [a.u.]
distance [nm]
D
Occurrence [%]
CBC
Non-activated
hCD47
hCD47 + hIgG
hIgG
E
NND [nm]
****
ns
-
hCD47
hCD47 + hIgG
hIgG
F
Occurrence [%]
Centroid NN distance [nm]
Non-activated
hCD47
hCD47 + hIgG
hIgG
G
Occurrence [%]
CBC
Non-activated
hCD47
hCD47 + hIgG
hIgG
H
NND [nm]
**
***
****
-
hCD47
hCD47 + hIgG
hIgG
I
Occurrence [%]
Centroid NN distance [nm]
Non-activated
hCD47
hCD47 + hIgG
hIgG

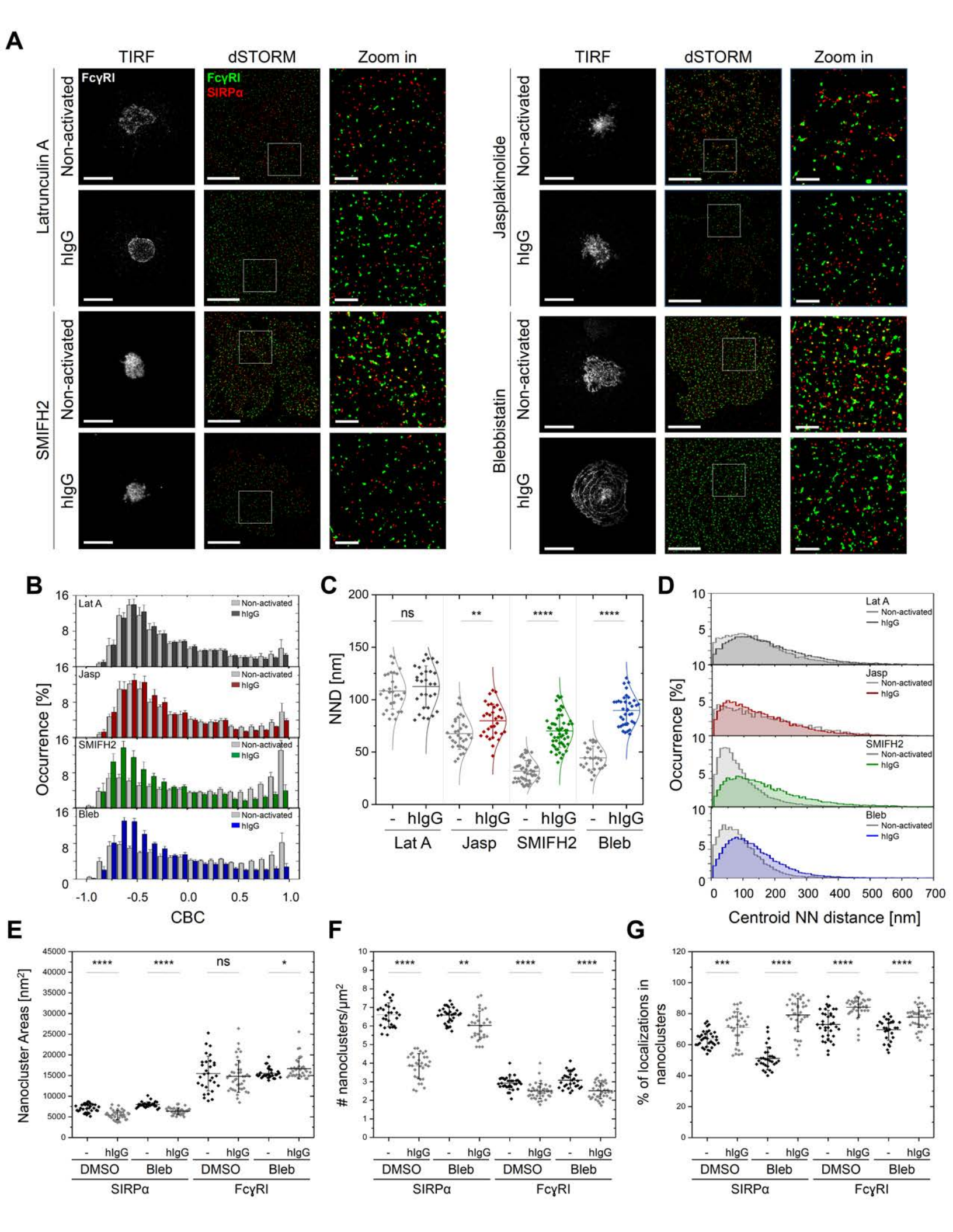
A
TIRF
dSTORM
Zoom in
FcγRI
FcγRI
SIRPα
Latruncullin A
Jasplakinolide
Blebbistatin
SMIFH2
Non-activated
hIgG
B
Lat A
Jasp
SMIFH2
Bleb
Non-activated
hIgG
Occurrence [%]
CBC
C
NND [nm]
ns
**
****
****
- hIgG
Lat A
Jasp
SMIFH2
Bleb
D
Occurrence [%]
Centroid NN distance [nm]
E
Nanocluster Areas [nm²]
****
****
ns
*
DMSO
Bleb
SIRPα
FcγRI
F
nanoclusters/µm²
****
**
****
****
G
% of localizations in nanoclusters
***
****
****
****

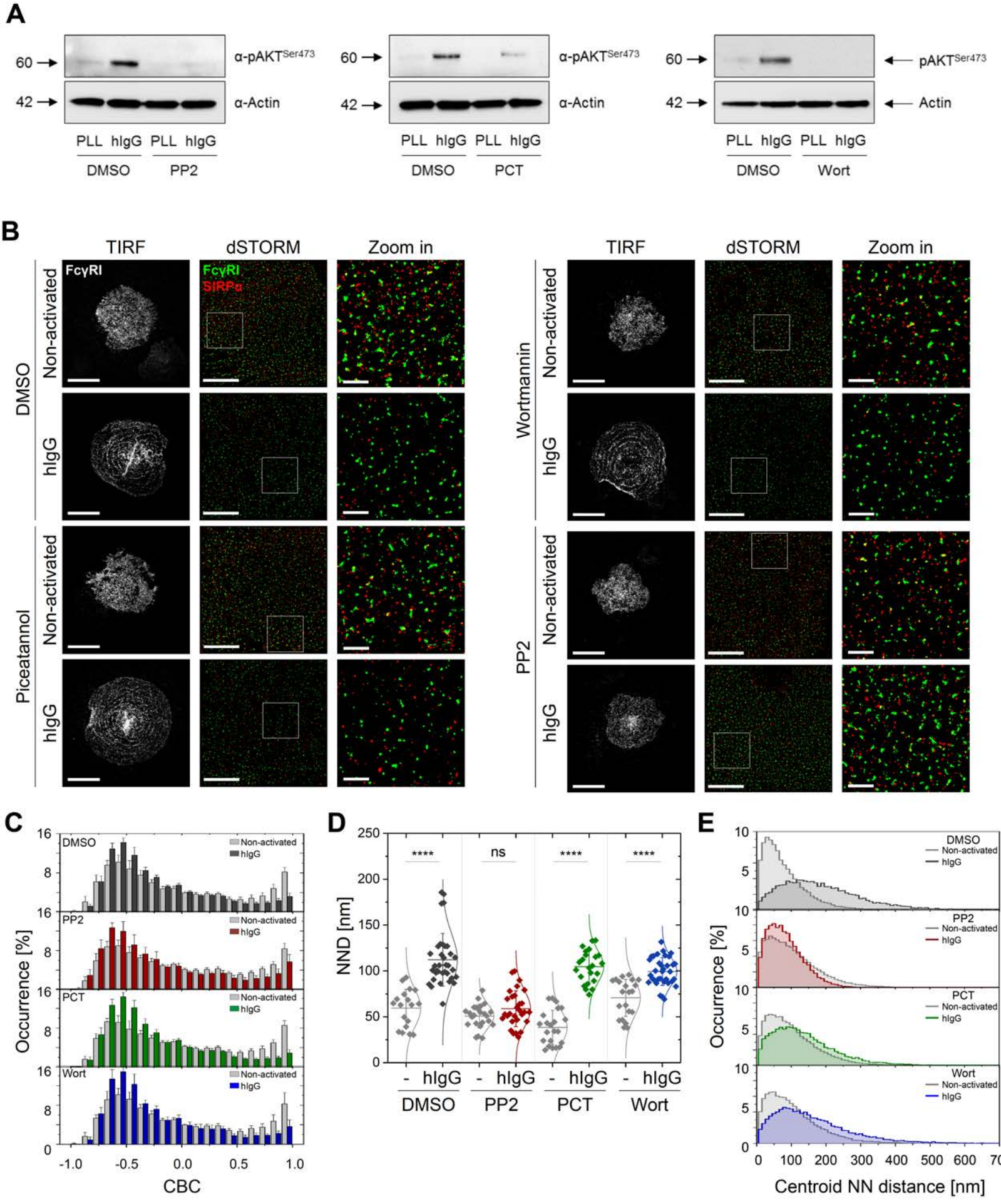
A
60
42
α-pAKTSer473
α-Actin
PLL hIgG PLL hIgG
DMSO PP2
DMSO PCT
pAKTSer473
Actin
DMSO Wort
B
TIRF
dSTORM
Zoom in
FcγRI
SIRPα
DMSO
Piceatannol
Wortmannin
PP2
Non-activated
hIgG
C
Occurrence [%]
CBC
DMSO
PP2
PCT
Wort
Non-activated
hIgG
D
NND [nm]
****
ns
E
Centroid NN distance [nm]

Supplemental Figure Legends

Figure S1. Phenotype of macrophages and analysis of SIRPα, FcγRI and FcγRII surface expression.

(A) Primary human macrophages were stained for different surface markers as indicated and analyzed by flow cytometry. For each marker, specific staining (grey histogram) is compared with an isotype-matched control staining (black open histogram). (B-D) Cells were incubated for 10 or 30 min in wells coated with PLL (non-activated) or hIgG, stained and analyzed by flow cytometry. Expression of SIRPα (B), FcγRI (C) and FcγRII (D) in the live $CD14^+$ cells was assessed with APC-labeled specific antibodies (B and C) or with unlabeled primary antibody followed by isotype-specific secondary antibody conjugated with AF488 (D). For each receptor, representative histograms of specific staining (grey and black dashed open histogram) are compared with an isotype-matched control (black open histogram). Bars represent the geometric mean fluorescence intensity (gMFI) ± SD of 3 independent donors.

Figure S2. Nanometre-scale organization of SIRPα and FcγRI at 30 min of stimulation.

(A and B) Representative TIRF and dSTORM images of SIRPα (A) and FcγRI (B) at the surface of primary human macrophages seeded onto PLL (non-activated, top row) or hIgG-coated slides (bottom row) for 30 min, and stained with fluorescently labeled specific antibodies. Scale bars represent 5 µm. The regions delineated by the white squares are zoomed-in and shown with corresponding density maps and binary maps. Scale bars represent 1 µm. (C) Nanocluster areas, (D) density, and (E) percentage of localizations in nanoclusters for SIRPα and FcγRI under non-activated (black) or hIgG-activated (grey) conditions were calculated as in Figure 1. (F) Representative TIRF and dSTORM images showing FcγRI (green) and SIRPα (red) at the surface of primary human macrophages incubated for 30 min as in (A) and (B), and stained with anti-FcγRI-AF488 and anti-SIRPα-AF647 mAbs. Scale bars represent 5 µm. Regions outlined by the white squares (middle column) are shown enlarged (right columns) with relative fluorescence intensity profiles

along the white lines. Scale bars represent 1 µm. (G) CBC histograms of the single-molecule distributions of the co-localization parameter for FcγRI and SIRPα in cells seeded onto PLL- (light grey) or hIgG-coated (light red) slides, or in positive control (green). The positive control data in this figure is the same as in Figure 2. Data are from a minimum of 30 cells from 3 independent donors. Bars represent mean ± SD. (H) NND analysis from data shown in (G). Each symbol represents the median NND of all paired single-molecule localizations from one cell. Horizontal lines and error bars represent mean ± SD. Data are from a minimum of 30 cells from 3 independent donors. ns, not significant. **($p<0.01$), ****($p<0.0001$), two-tailed t-test assuming unequal variance. (I) Histogram distributions of the NND between the centroids of nanoclusters from one channel and the centroid of their nearest neighbor from the second channel (≥ 20,000 clusters from a minimum of 10 cells per condition) in PLL (light grey), hIgG (light red) or positive control (green) conditions.

Figure S3. FcγRI reorganization into concentric rings at the phagocytic synapse visualized by confocal microscopy.

(A and B) Representative confocal image of FcγRI at the phagocytic synapse and XZ and YZ orthogonal sections. Cells were allowed to spread onto PLL- (A) or hIgG-coated (B) slides for 10 min, fixed and stained with an anti-FcγRI mAb conjugated with AF488 (green), the membrane dye DiD (red), and NucBlue® Live cell stain (blue) to visualize the nucleus. Z-depth for non-activated and hIgG conditions is 13 µm and 10 µm, respectively. Scale bars represent 10 µm. See also Video 3 and 4. (C) Isotype-matched control staining. Representative bright-field (scale bars represent 10 µm), and TIRF and dSTORM images (scale bars represent 5 µm) corresponding to the regions outlined by the white squares, showing primary human macrophages stained with isotype-matched control antibodies for all antibodies used throughout this study.

Figure S4. Engagement of Fcγ receptors is required for their reorganization into concentric rings.

(A and B) Representative TIRF (scale bars represent 10 μm) and dSTORM images (scale bars represent 5 μm) showing FcγRI (green) and FcγRII (red), at the surface of primary human macrophages, incubated for 10 min (A) or 30 min (B) on slides coated with hIgG1 or hIgG2, and stained with anti-FcγRI-AF488 and anti-FcγRII-AF647 mAbs. In each condition, regions outlined by the white squares (middle column) are shown enlarged (right column) with relative fluorescence intensity profiles along the white lines. Scale bars represent 1 μm. (C) CBC histograms of the single-molecule distributions of the co-localization parameter for FcγRI and FcγRII in cells seeded onto hIgG1- or hIgG2-coated slides for 10 (light grey and dark grey, respectively) or 30 min (light red and dark red, respectively). Data are from a minimum of 30 cells from 3 independent donors. Bars represent mean ± SD. (D) NND analysis from data shown in (C). Each symbol represents the median NND of all paired single-molecule localizations from one cell. Horizontal lines and error bars represent mean ± SD. ns, not significant. ****($p<0.0001$), one-way ANOVA with Tukey's post-hoc test. (E) Histogram distributions of the NND between the centroids of nanoclusters from one channel and the centroid of their nearest neighbor from the second channel (≥ 10,000 clusters from a minimum of 10 cells per condition).

Figure S5. SIRPα inhibition of FcγRI segregation and reorganization into concentric rings persists at 30 min of activation.

(A) Representative TIRF images of FcγRI at the surface of primary human macrophages incubated for 30 min on slides coated with hCD47 or hCD47 + hIgG, and stained with a fluorescently labeled specific antibody. Scale bars represent 10 μm. (B) Representative TIRF and dSTORM images showing FcγRI (green) and SIRPα (red) at the surface of primary human macrophages incubated for 30 min on slides coated with hCD47 (top row) or hCD47 + hIgG (bottom row), and stained with anti-FcγRI-AF488 and anti-SIRPα-AF647 mAbs. Scale bars represent 5 μm. In each condition, regions outlined by the white squares (middle column) are shown enlarged (right column) with relative fluorescence intensity profiles along the white lines. Scale bars represent 1 μm. (C) CBC histograms of the single-

molecule distributions of the co-localization parameter for FcγRI and SIRPα in cells seeded onto slides coated with PLL (light grey), hCD47 (light red), hCD47 + hIgG (dark red) or hIgG (dark grey) for 30 min. Data are from a minimum of 30 cells from 3 independent donors. Bars represent mean ± SD. (D) NND analysis from data shown in (C). Each symbol represents the median NND of all paired single-molecule localizations from one cell. Horizontal lines and error bars represent mean ± SD. ns, sot significant. ****($p<0.0001$), one-way ANOVA with Tukey's post-hoc test. (E) Histogram distributions of the NND between the centroids of nanoclusters from one channel and the centroid of their nearest neighbor from the second channel (≥ 10,000 clusters from a minimum of 10 cells per condition).

Supplemental Videos

Video 1. Live TIRF imaging of the distribution of FcγRI at the cell surface during the spreading of live primary human macrophages under non-activating conditions (frame rate, 10 frames/s, sped up 20x from real time). Scale bars represent 10 μm for full cell and 2 μm for inset image.

Video 2. Live TIRF imaging of the formation of FcγRI concentric rings at the cell surface during the spreading of live primary human macrophages under activating conditions (frame rate, 5 frames/s, sped up 20x from real time). Scale bars represent 10 μm for full cell and 2 μm for inset image.

Video 3. The video shows a representative confocal Z-stack and 3D projection of the distribution of FcγRI at the surface of primary human macrophages under activating conditions. FcγRI (green); cell membrane (red); nucleus (blue). Scale bar represents 10 μm.

Video 4. The video shows a representative confocal Z-stack and 3D projection of the distribution of FcγRI at the surface of primary human macrophages under non-activating conditions. FcγRI (green); cell membrane (red); nucleus (blue). Scale bar represents 10 μm.

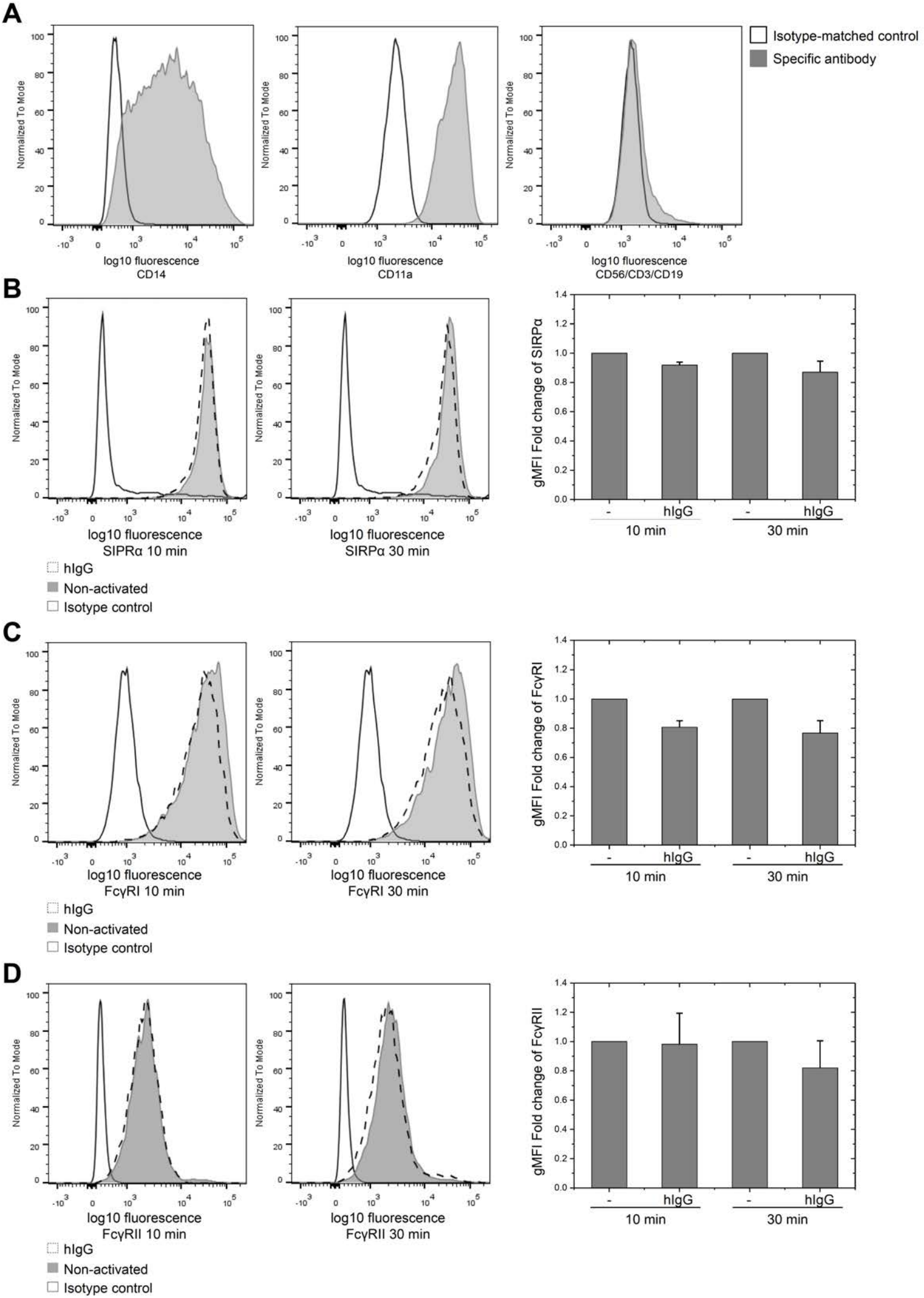
A
Isotype-matched control
Specific antibody
Normalized To Mode
log10 fluorescence
CD14
log10 fluorescence
CD11a
log10 fluorescence
CD56/CD3/CD19
B
log10 fluorescence
SIPRα 10 min
log10 fluorescence
SIRPα 30 min
gMFI Fold change of SIRPα
hIgG
Non-activated
Isotype control
10 min
30 min
C
log10 fluorescence
FcγRI 10 min
log10 fluorescence
FcγRI 30 min
gMFI Fold change of FcγRI
D
log10 fluorescence
FcγRII 10 min
log10 fluorescence
FcγRII 30 min
gMFI Fold change of FcγRII

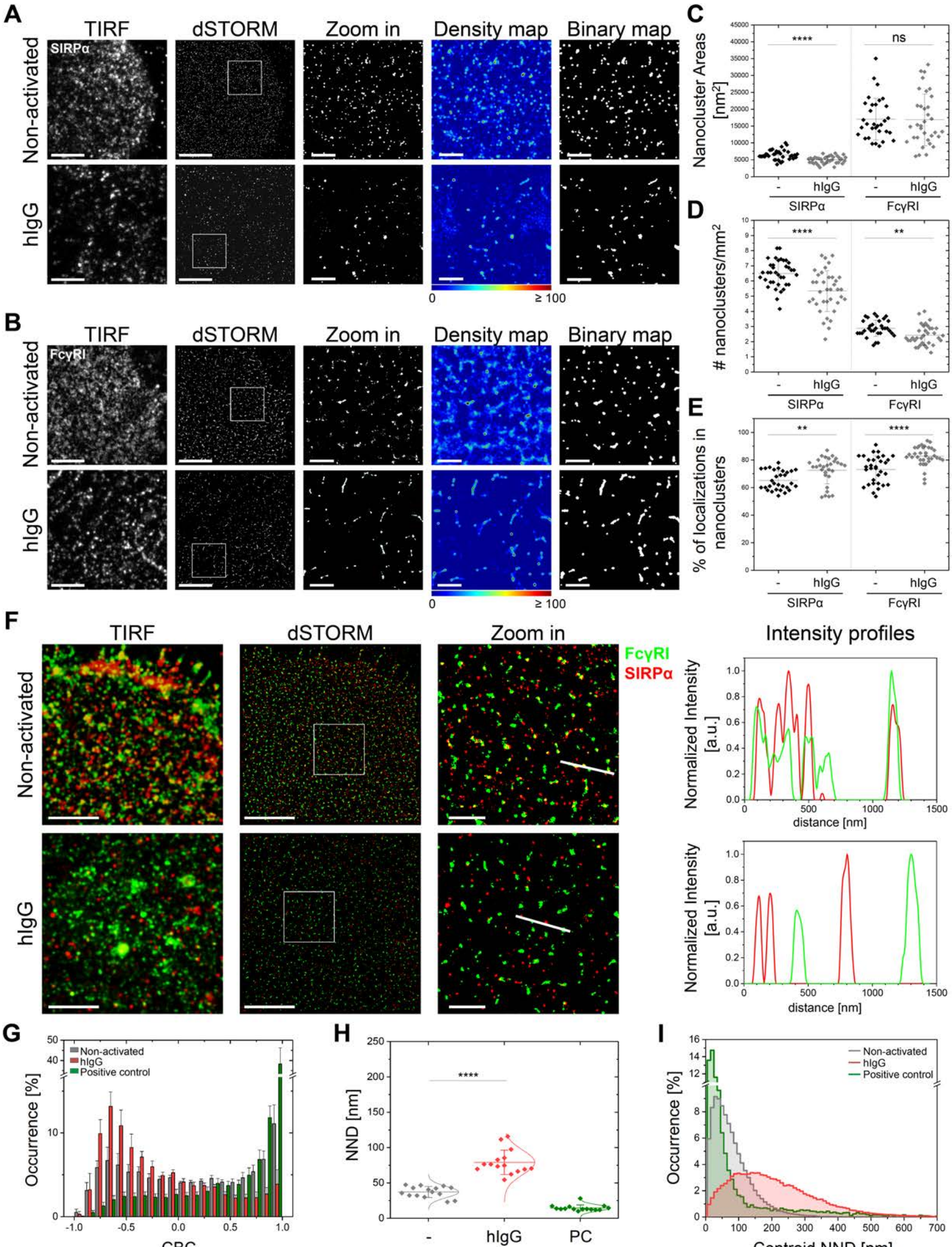
A
TIRF
dSTORM
Zoom in
Density map
Binary map
SIRPα
Non-activated
hIgG
0
≥ 100
B
FcγRI
C
Nanocluster Areas [nm²]
****
ns
-
hIgG
SIRPα
FcγRI
D
nanoclusters/mm²
****
**
E
% of localizations in nanoclusters
**
****
F
FcγRI
SIRPα
Intensity profiles
Normalized Intensity [a.u.]
distance [nm]
G
Non-activated
hIgG
Positive control
Occurrence [%]
CBC
H
NND [nm]
****
PC
I
Centroid NND [nm]

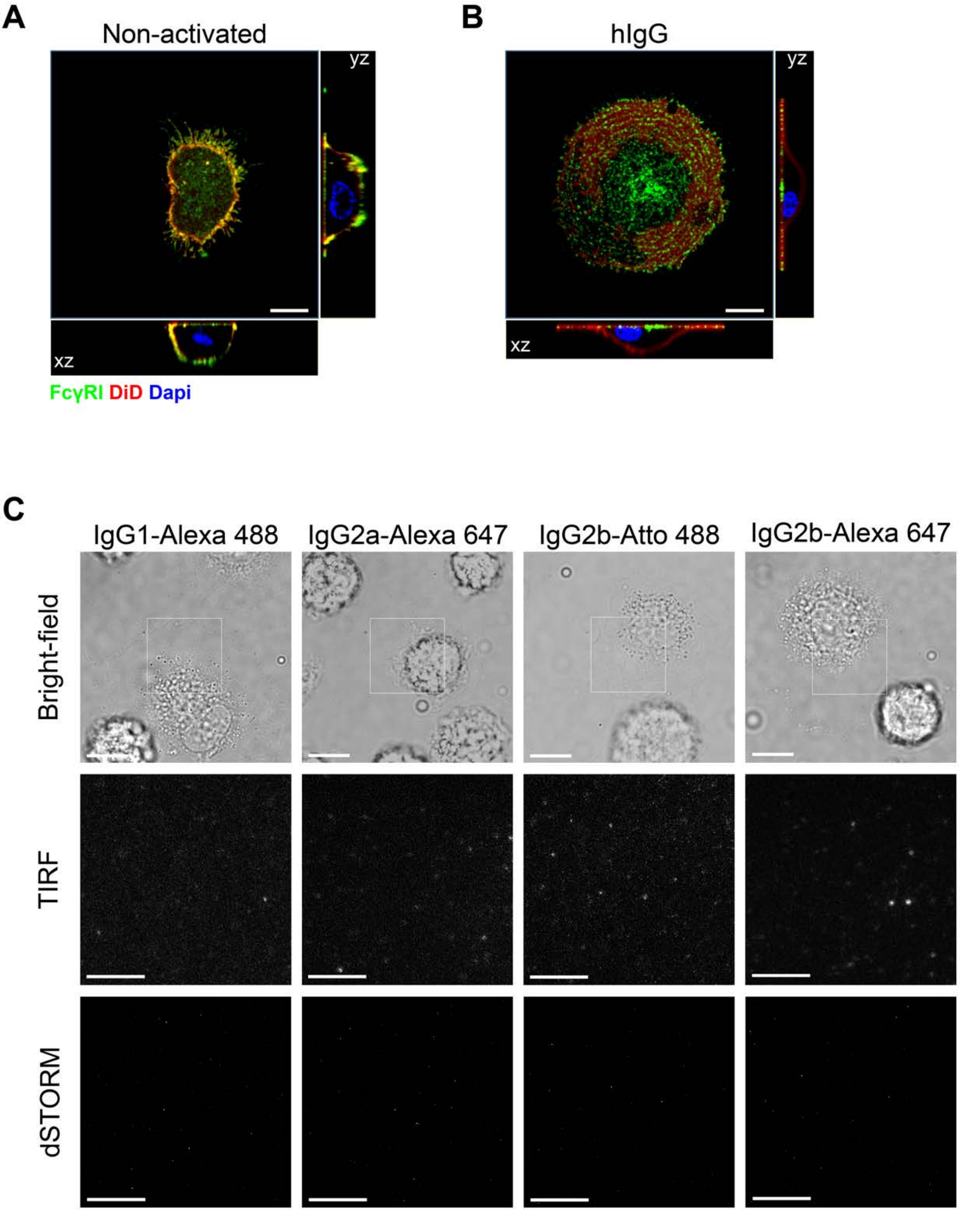
A
Non-activated
yz
xz
FcγRI DiD Dapi
B
hIgG
yz
xz
C
IgG1-Alexa 488
IgG2a-Alexa 647
IgG2b-Atto 488
IgG2b-Alexa 647
Bright-field
TIRF
dSTORM

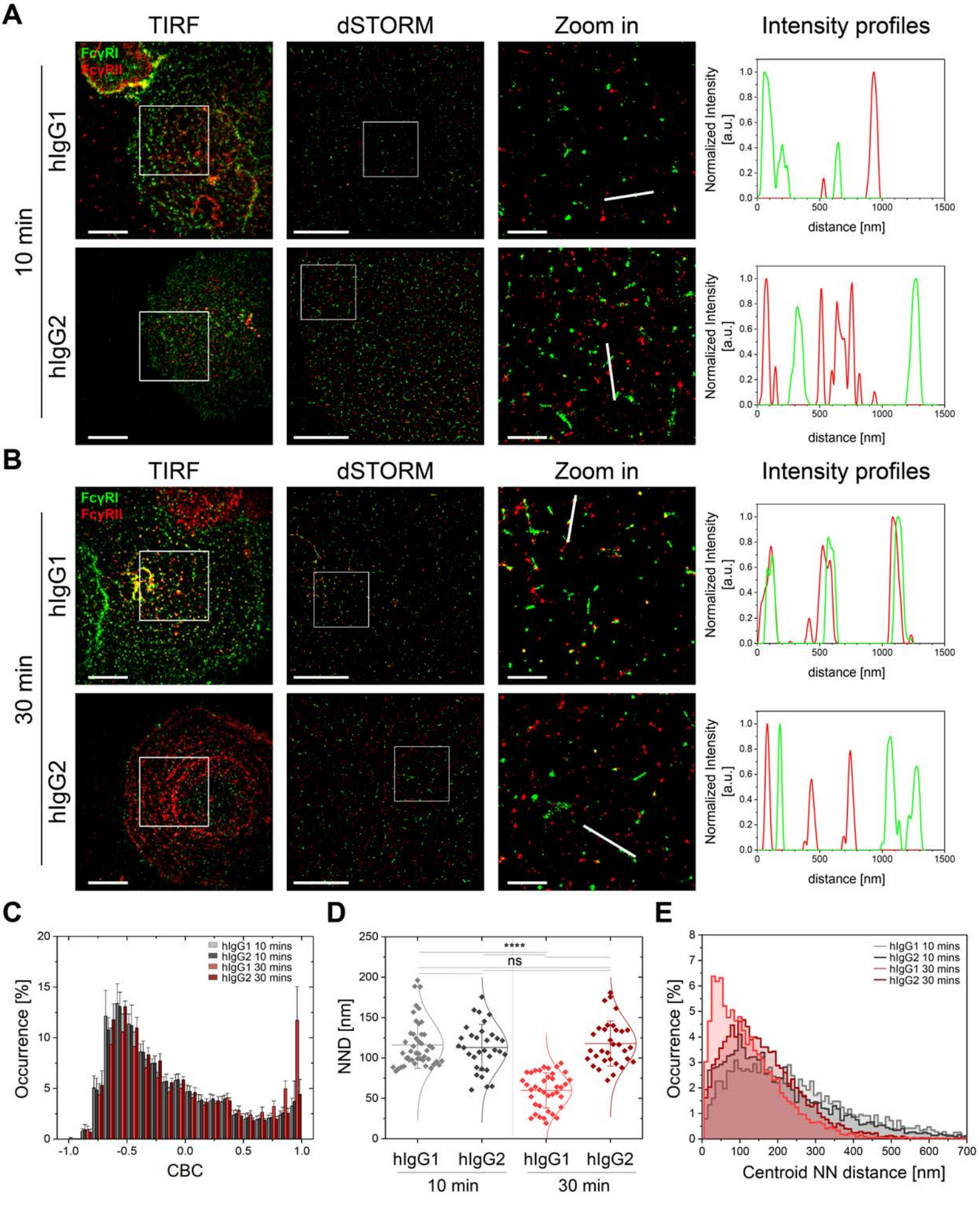
A
TIRF
dSTORM
Zoom in
Intensity profiles
FcγRI
FcγRII
10 min
hIgG1
hIgG2
Normalized Intensity [a.u.]
distance [nm]
B
30 min
C
Occurrence [%]
CBC
hIgG1 10 mins
hIgG2 10 mins
hIgG1 30 mins
hIgG2 30 mins
D
NND [nm]
****
ns
hIgG1
hIgG2
hIgG1
hIgG2
10 min
30 min
E
Occurrence [%]
Centroid NN distance [nm]

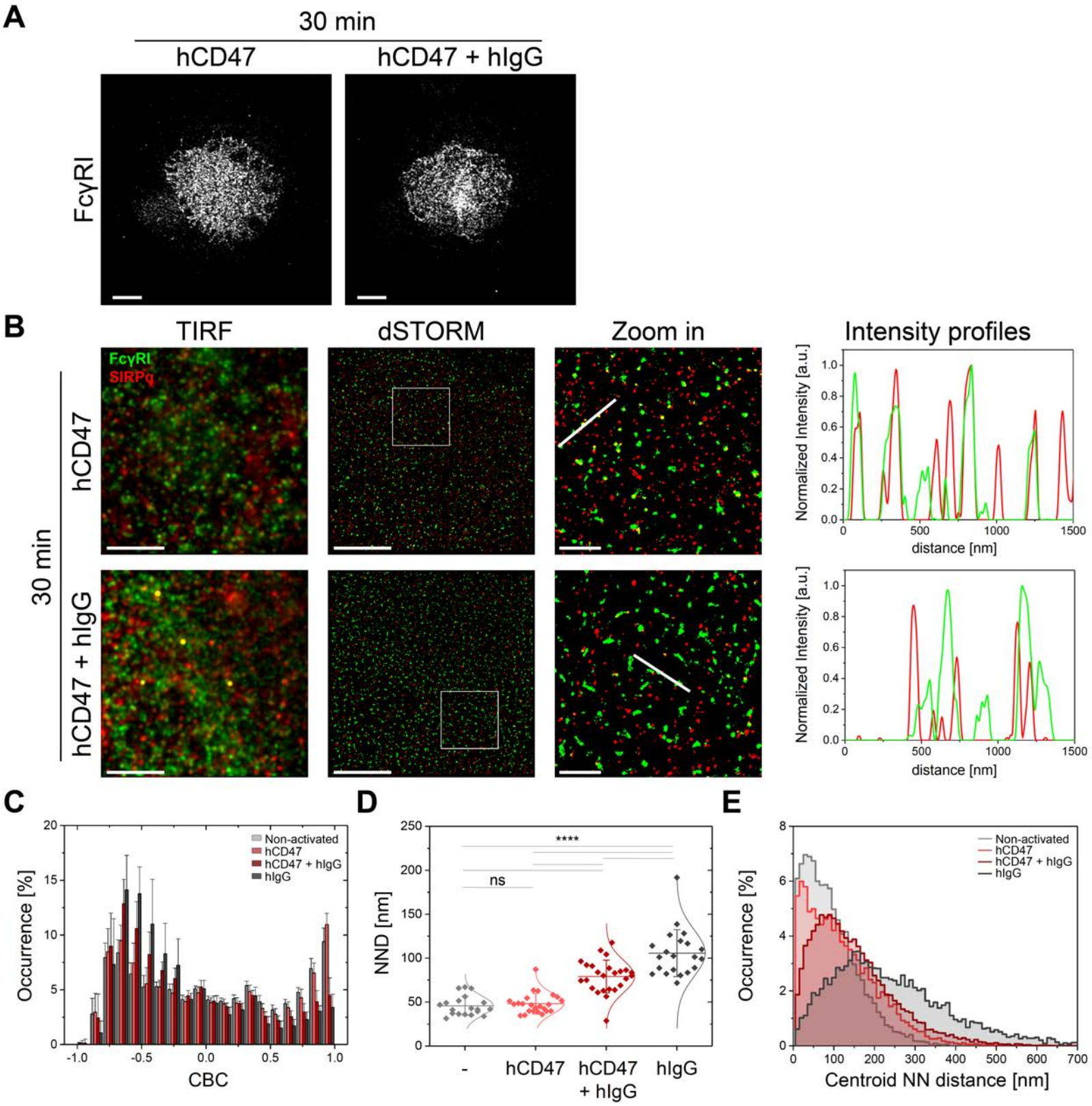
A
30 min
hCD47
hCD47 + hIgG
FcγRI
B
TIRF
dSTORM
Zoom in
Intensity profiles
FcγRI
SIRPα
hCD47
hCD47 + hIgG
30 min
Normalized Intensity [a.u.]
distance [nm]
C
Non-activated
hCD47
hCD47 + hIgG
hIgG
Occurrence [%]
CBC
D
NND [nm]
****
ns
-
hCD47
hCD47 + hIgG
hIgG
E
Non-activated
hCD47
hCD47 + hIgG
hIgG
Occurrence [%]
Centroid NN distance [nm]